School of Physics & Astronomy
Queen Mary University of London

Basic Description of the Cosmic Microwave Background Radiation

Dong Ha Lee (220269735)

Supervised by Dr Karim Malik

Submitted August 2023 for module SPA7000P in partial fulfilment
of the requirements for the degree of
MSc Astrophysics at Queen Mary University of London

Declaration

I hereby certify that this Dissertation, which is approximately 14 thousand words in length, has been written by me at the School of Physics and Astronomy, Queen Mary University of London, that all material in this dissertation which is not my own work has been properly acknowledged, and that it has not been submitted in any previous application for a higher degree.

All figures and diagrams are produced by the author unless explicitly stated otherwise. The derivations and results in Section 2 unless stated otherwise have been derived with guidance mainly from Theoretical Astrophysics Vol.1 & 3 by T. Padmanabhan. The derivations in Section 3 mainly follows the lecture notes of Dr K. Malik on Advanced Cosmology at Queen Mary university of London and Dr Hannu Kurki-Suonio of the Univeristy of Helsinki. This dissertation attempts to reproduce results and derivations from various sources on the different aspects of the Cosmic Microwave Background Radiation. Any results in derivation of the different aspects of the CMBR which are not explicitly stated are my own work of a reproduction and re-derivation of a stated result in a given source.

Dong Ha Lee (220269735)

Acknowledgements

I would like to thank Dr Karim Malik for supervising my project and putting up with all the last minute changes and uncertainty though the project due to my own doing. I would also like to thank my family, particularly my gradparents for helping me through my sudden stay in Korea. Finally, I would like to thank the kind people at Yonsei University in Seoul for allowing me access to their library.

Abstract

This dissertation attempts to describe the basic parameters of the Cosmic Microwave Background, starting from the cause of the decoupling event itself and touching on the cause of the perturbations of the largely isotropic radiation field.

The formation of the microwave background was due to the freeze-out of the interaction between light and matter as the universe cooled with time. We consider the conditions for hydrogen recombination which accelerates this process and attempt to verify whether the models used are physically valid and attempt to reproduce the evolution of the ionisation fraction simulated by CAMB. We show that the recombination rate is less than that of the Saha model and find the redshift at which Thomson scattering freezes out to be $z = 743.4$.

This dissertation also attempts to cover the idea of cosmological perturbation theory and how it can be used to explain the sources of anisotropy in the CMB. We derive the equation for the Sachs-Wolfe effect in Newtonian gauge at linear order of scalar metric perturbations.

Contents

List of Figures

List of Tables

1 Introduction

1.1 Conventions

In this Dissertation, we will occasionally interchange between several conventions and units but most quantities will largely be represented in Gaussian CGS units. This will particularly be the case when discussing hydrogen recombination in Chapter 2.

For convenience, thermal (k_BT) and mass (mc^2 but less so in order to keep track of dimensions when calculating atomic quantities) energy terms will occasionally be listed without the respective constant terms.

Any source of potential confusion or changes in convention will be, more often than not, explicitly stated and clarified.

1.2 Cosmology

Cosmology is the study of the evolution of the universe. This section will attempt to introduce the fundamental properties of the universe and its evolution. This will aid us in describing the universe and it's properties as it leads up to a a specific moment in this universe's history: a phenomenon referred to as the decoupling of light and matter (or the formation of the Cosmic Microwave Background).

The cosmological principle states that on large scales, the universe is homogeneous and isotropic. This universe can be described by the Friedmann-Robertson-Walker (FRW) metric

$$\mathrm{d}s^2 = -\mathrm{d}t^2 + a^2(t)\left(\frac{\mathrm{d}r^2}{1-kr} + r^2\mathrm{d}\theta^2 + r^2 sin^2\theta \mathrm{d}\phi^2\right) \tag{1.1}$$

under the (-,+.+,+) convention (Malik (2022)) and using $c = 1$. Where t is the cosmic time of the universe, (r, θ, ϕ) are the dimensionless, spatial comoving coordinates which are independent of the expansion of the universe where r is the radial, comoving length in the metric. These comoving coordinates are related to physical

coordinates by the scale factor $a(t)$ which encapsulates the expansion.

The spacetime defined by the FRW metric (Equation 1.1) evolves according to the Friedmann equations (Malik 2022)

$$H^2 = \left(\frac{\dot{a}}{a}\right)^2 = \frac{8\pi G\rho(t)}{3} - \frac{k}{a^2} + \frac{\Lambda}{3} \tag{1.2}$$

and

$$\frac{\ddot{a}}{a} = -\frac{4\pi G}{3}(\rho + 3p) + \frac{\Lambda}{3} \tag{1.3}$$

where we have defined the Hubble parameter $H = \dot{a}/a$, ρ is the mass density, k is the spatial curvature parameter, p is the pressure and Λ is the cosmological constant. To solve these equations, the equation of state is required. This is defined by

$$p = w\rho \tag{1.4}$$

where w is the equation of state parameter and is usually considered to be constant in time for all species in the standard cosmological model.

Using Equations 1.2 and 1.3, we can find how the density of different species changes with the scale factor. Taking the derivative with respect to time of equation 1.2 gives

$$2H\left(\frac{\ddot{a}}{a} - H^2\right) = \frac{8\pi G\dot{\rho}}{3} + \frac{k}{a^2} \tag{1.5}$$

which can be substituted into Equation 1.3 to give

$$\dot{\rho} = -3H(\rho + p) \tag{1.6}$$

which is the energy conservation equation. Substituting Equation 1.4 into this equation and integrating, we find that the density evolves as

$$\rho = \rho_0 \left(\frac{a}{a_0}\right)^{-3(1+w)} \tag{1.7}$$

with the scale factor a. Where ρ_0 and a_0 are the density and scale factor evaluated at $t = t_0$ which is the present time.

Substituting Equation 1.7 into the Friedmann equation (Equation 1.2) for each of the different species of particles of the universe of given w allows us to solve for how the scale factor evolves with time. This in full generality must be solved numerically.

However, as the density of species of different w have different dependencies on a, one can make the reasonable assumption that at different points in this universe's

history, a different term on the right hand side (RHS) of Equation 1.2 would have been the dominant term in that corresponding phase of the universe. This simplified equation can be solved for non-relativistic matter ($w = 0$), ultra-relativistic matter ($w = 1/3$), the curvature term ($-k/a^2$) and the cosmological constant term ($\Lambda/3$) using boundary conditions of $a(t_0) = a_0$ and $a(0) = 0$.

Substituting Equation 1.7 with the relevant w into the Friedmann equation shows that the radiation density initially dominates due to it's high, $\propto a^{-4}$ dependence but falls away quickly to matter domination (a^{-3}), then curvature (a^{-2}) and finally entering the cosmological constant (constant) dominant phase which we reside in today. The evolution at each phase is summarised below in Table 1.1.

Table 1.1: Analytical solutions for Equation 1.2 at each phase of the universe. For the Λ dominated phase, we cannot set initial conditions to be $a(0) = 0$.

Phase	w	$H^2(a)$	$a(t)$	$H(t)$
Radiation	$\frac{1}{3}$	$\frac{8\pi G\rho_0}{3}\left(\frac{a}{a_0}\right)^{-4}$	$a_0\left(\frac{t}{t_0}\right)^{1/2}$	$\frac{1}{2t}$
Matter	0	$\frac{8\pi G\rho_0}{3}\left(\frac{a}{a_0}\right)^{-3}$	$a_0\left(\frac{t}{t_0}\right)^{2/3}$	$\frac{2}{3t}$
Curvature	$-\frac{1}{3}$	$-\frac{k}{a^2}$	$a_0\frac{t}{t_0}$	$\frac{1}{t}$
Λ	-1	$\frac{\Lambda}{3}$	$a_0\exp\left[\sqrt{\frac{\Lambda}{3}}(t-t_0)\right]$	$\sqrt{\frac{\Lambda}{3}}$

More detailed solutions of full generality cannot be solved analytically and must be approached numerically. For this purpose, a polynomial form of Equation 1.2 will prove to be more useful.

We begin by considering the redshift of a photon with emitted frequency of ν defined by

$$z + 1 = \frac{\nu}{\nu_0} \tag{1.8}$$

where ν_0 is the frequency of the observed photon after being redshifted by z. By considering time intervals at the emitter and observer for radially ($d\theta = d\phi = 0$) travelling photons ($ds = 0$), one can derive the following relation between the scale factor and the redshift (Pritchard 2016)

$$1 + z = \frac{a_0}{a} \tag{1.9}$$

where $a_0 = a(t_0)$.

We can also define the critical density $\rho_c = 3H_0^2/8\pi G$ as the total present-day density required to have the currently observed Hubble constant (H_0) for a universe of zero curvature and cosmological constant ($k = \Lambda = 0$). We can also rewrite the Hubble parameter as $H = H_0E(z)$ where $E(z)$ is the Hubble function. This Hubble

function encapsulates the time dependence of the Hubble parameter. The Hubble function is a dimensionless quantity which we can define using Equation 1.2 as

$$E^2(z) = \frac{\rho(z)}{\rho_c} - \frac{k(1+z)^2}{a_0^2 H_0^2} + \frac{\Lambda}{3H_0} \tag{1.10}$$

where we have also used the critical density ρ_c.

To find $\rho(z)$, we can use the equation of state parameters given in Table 1.1 for pressure-less, non-relativistic matter ($w = 0$) and radiation ($w = 1/3$). Inserting these parameters into Equation 1.7 gives $\rho_m = \rho_{m,0}(a/a_0)^{-3}$ and $\rho_r = \rho_{r,0}(a/a_0)^{-4}$ respectively. We can then substitute for the redshift using Equation 1.9 and define the density parameter of species i to be $\Omega_i = \rho_{i,0}/\rho_c$ where we can define $\rho_{k,0} = -3k/8\pi a_0^2 G$ and $\rho_{\Lambda,0} = \Lambda/8\pi G$ for curvature and cosmological constant equivalent densities respectively.

Hence, Equation 1.10 becomes

$$E^2(z) = \Omega_r(1+z)^4 + \Omega_m(1+z)^3 + \Omega_k(1+z)^2 + \Omega_\Lambda \tag{1.11}$$

The Hubble constant (H_0) has dimensions of [Time^{-1}] and is the Hubble parameter ($H = \dot{a}/a$) evaluated at the present time ($t = t_0$) and can be written in the form

$$H_0 = 100h\,\mathrm{km}\cdot\mathrm{s}^{-1}\cdot\mathrm{Mpc}^{-1} = 3.241\times10^{-18}h\,\mathrm{s}^{-1} \tag{1.12}$$

where h is a dimensionless parameter of order unity (between 0.6 0.8 depending on the method used to obtain the constant).

The main source of this uncertainty in h is due to what is known as the Hubble tension. This is where the measurements of the Hubble constant assuming a flat, cold dark matter (ΛCDM) universe differs by $\sim 4\sigma$ between early and late universe measurements (Riess et al. 2021).

A measurement of H_0 by Balkenhol et al. (2022) using the CMB power spectrum obtained values of $68.1 \pm 0.74\,\mathrm{km}\cdot\mathrm{s}^{-1}\cdot\mathrm{Mpc}^{-1}$ while type 1a Supernovae (SNe) Pantheon+ analysis (Brout et al. 2022) obtained values of $73.6 \pm 1.1\,\mathrm{km}\cdot\mathrm{s}^{-1}\cdot\mathrm{Mpc}^{-1}$. Figure 1.1 reveals how this H_0 discrepancy affects the Hubble parameter at different times. The Hubble parameters resulting from the respective observations result in significant deviation from one another as we go further back in time.

Due to such uncertainties in measured parameters (especially due often due to their dependence on H_0), Table 1.3 is presented below to indicate the values of key observed parameters of our universe which are used in this dissertation unless

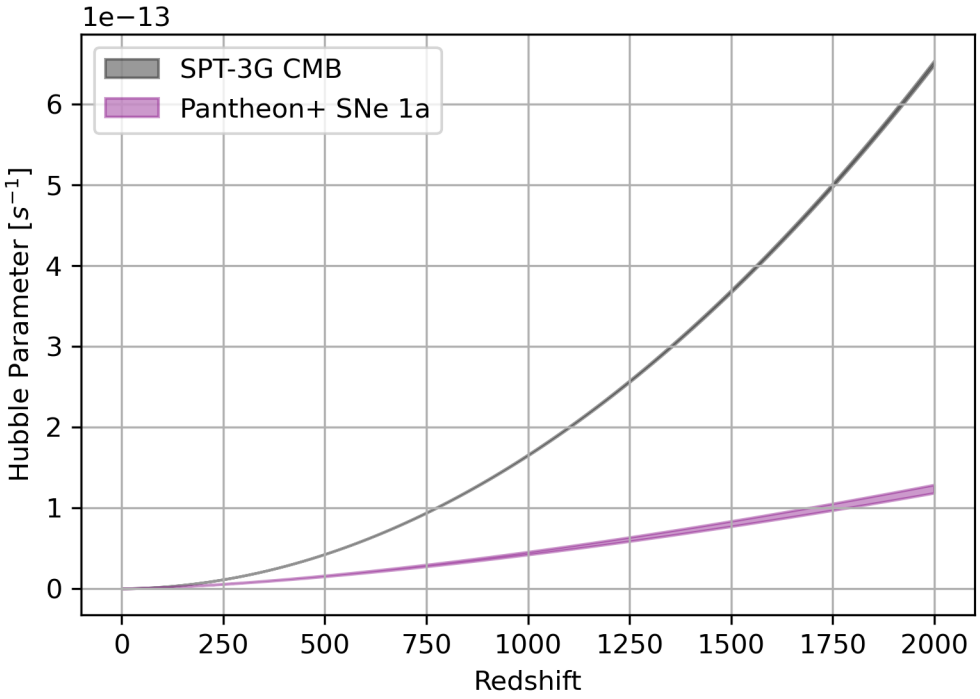

Figure 1.1: Evolution of the Hubble parameter for measurements of H_0 and the density parameters in Table 1.2. The difference between the two graphs at $z = 1100$ is $(1.49 \pm 0.03) \times 10^{-13}\,\mathrm{s}^{-1}$. Figure produced by the author using parameters given by Balkenhol et al. (2022) and (Brout et al. 2022). All figures in this dissertation are self produced unless stated explicitly otherwise.

Table 1.2: Cosmological parameters measured by Balkenhol et al. (2022) and Brout et al. (2022) for a flat ΛCDM universe. $\Omega_k = 0$ and $\Omega_r = 1 - \Omega_\Lambda - \Omega_m$.

Phenomena	H_0 [km·s^{-1}·Mpc^{-1}]	Ω_Λ	Ω_m
CMB	68.1 ± 0.74	0.6894 ± 0.0076	$(0.14334 \pm 0.0026)/h^2$
SNe 1a	73.6 ± 1.1	0.666 ± 0.018	0.334 ± 0.018

specified otherwise.

Table 1.3: List of parameters to be used in calculations in this dissertation (taken from Groom).

Quantity	Symbol	Value
Current CMB temperature	T_0	$2.7255\,\mathrm{K}$
Baryon to photon ratio	η	6.05×10^{-10}
Hubble constant factor	h	0.673
CMB density parameter	Ω_r	$2.473 \times 10^{-5} h^{-2}$
Non-relativistic matter density parameter	Ω_m	$0.14187 h^{-2}$
Dark energy density parameter	Ω_Λ	0.685

Some of these quantities are yet to be formally defined but will be when used.

1.3 Cosmic Microwave Background Radiation

The Cosmic Microwave Background (CMB) radiation is a near perfect isotropic blackbody radiation field which pervades the universe with a mean temperature of 2.725 K. As the CMB can be modelled as a blackbody, to understand how the current parameters of the CMB came to be as they are today, we can look at how a blackbody changes under the expansion of the universe. The energy density of a blackbody of temperature T in range $[\nu, \nu + \mathrm{d}\nu]$ inside a physical volume ($\propto a^3 \propto (1+z)^{-3}$) is

$$u(\nu, T) = \frac{8\pi h}{c^3} \frac{\nu^3}{e^{h\nu/T} - 1} \tag{1.13}$$

We can substitute Equation 1.8 to find that the energy density of photons coming from redshift z across an expanding volume equal to the expansion of the universe is related to the original energy density by

$$u(\nu, T) = (1+z)^3 u(\nu_0, T/(1+z)) \tag{1.14}$$

where the energy density on the right hand side is the energy density measured today (Pritchard 2016). This shows that the comoving number density of photons is constant and that the effective temperature of a blackbody is related to the redshift by

$$T(z) = T_0(1+z) \tag{1.15}$$

where T_0 would be the effective temperature of the blackbody at present time (2.725 K for the CMB).

For all interacting species in an expanding universe, the physical number density

falls with the expansion. Therefore, while the different species may have been initially in thermodynamic equilibrium with one another due to collisions, they will reach a point where the rates of interactions with other species falls below the expansion rate of the universe. Beyond this point, the species is no longer in equilibrium with the rest of the universe and the properties of this species will only be affected by the universal expansion. This is known as freeze-out.

For photons, this freeze-out (or decoupling from interactions with matter) occurred at a redshift of $z \sim 10^3$. From this point onward, the universe became transparent to photons, allowing them to effectively propagate freely until eventually being observed today as the CMB. As the decoupling moment is the final time of interaction between matter and radiation, The time of CMB formation is also known as the surface of last scattering. Beyond this point, the temperature of the photons evolved according to Equation 1.15.

To consider how and when this decoupling occurred, we must consider the different interactions of light and matter and the times at which they no longer became favourable. This analysis (carried out in Chapter 2) shows that there are three distinct but linked major events which occurs at similar redshifts. These phenomena combined result in the formation of the CMB.

Initially, in the coupled matter-radiation fluid, the matter was mostly ionised hydrogen (free electrons and protons). However, as the universe cooled, it became more energetically favourable to form neutral hydrogen in the reaction

$$p^+ + e^- \rightleftharpoons H + \gamma \tag{1.16}$$

known as recombination. Eventually, there is a point when the matter content of the universe rapidly shifts from an ionised to neutral state. However, after this point, the hydrogen recombination reaction soon freezes, leaving behind a small number of free-electrons.

The typical photon scattering cross-section is $\propto m^{-2}$. As electrons are much lighter than protons, it is the interactions between the free electrons which kept the photons coupled to matter.

However, the sudden drop in the number of free electrons due to recombination along with the expansion of the universe results in the freeze-out of interactions between free-electrons and photons. This is known as the surface of last scattering.

These phenomena almost act as a domino which each triggering the next and the combination of these effects ultimately results in the formation of the CMB.

Not all the liberated photons are truly free from all interactions as some are

affected by gravitational lensing and others do continue to interact with the residual free electrons past the last scattering surface but these are minimal to the large scale isotropic structure of the CMB. But these are negligible to the large number of liberated photons from this event.

When we observe the CMB, we can measure small anisotropies within. Some of these are caused by perturbations in the universe which existed at the last scattering surface. Studying and understanding these anisotropies gives us an indication of the perturbations and structure of the early universe.

As the universe before decoupling was opaque to photons, the CMB provides us with the earliest possible direct optical observations of this universe.

1.4 CAMB

In this dissertation, we will use the Code for the Anisotropies in the Microwave Background (CAM) which is a code to obtain the evolution of cosmic parameters given a cosmological model. This allows us to solve the collisional Boltzmann equation for free electrons, giving us an accurate picture of the nature of the background parameters leading up to the decoupling of light and matter.

The original goal of this dissertation was to use CAMB to understand the different aspects of the perturbations relating to the anisotropies in the CMB. However, the focus of this dissertation shifted during the project towards the formation of the CMB itself and the the recombination of hydrogen in the early universe.

2 Recombination and Decoupling

2.1 Hydrogen Recombination

In Section 1.3, we introduced the CMB and stated that the formation of the CMB is a consequence of three major events.

First, the baryonic matter initially composed mostly of free electrons and protons drastically shifts from being ionised to neutral in a process known as recombination.

Next, this recombination quickly freezes out to leave a small number of free electrons which are able to interact with photons to maintain thermal equilibrium.

Finally, this results in photon-electron interactions soon freezing out for photons to leave them decoupled from the matter and free to propagate through the now transparent universe.

Therefore, to consider the formation of the CMB in detail, we must understand these processes. This section will look at the process of hydrogen recombination described by Equation 1.16. We shall consider the recombination of free electrons and protons in thermal equilibrium to ground-state hydrogen atoms. In future sections, we shall discuss the consequences of this recombination process on the photon-matter fluid comprising the universe prior to recombination and whether this is a reasonable assumption to have when considering the recombination process which triggered the formation of the CMB.

As this interaction is a reversible process, we must begin by considering the reverse process: photoionisation.

In Padmanabhan (2000), the cross-section of photoionisation is given by

$$\sigma_{bf}(\omega) = \frac{2^9\pi^2}{3}\left(\frac{q^2}{\hbar c}\right) a_0^2 \left(\frac{B}{\hbar\omega}\right)^4 \frac{\exp(-4\mu\,\mathrm{arccot}\mu)}{1-\exp(-2\pi\mu)} \tag{2.1}$$

where the subscript bf stands for bound-free interactions, q is the electron charge, m is the mass of the electron, ω is the angular frequency of ionising photons, B is

the ground-state energy of the hydrogen atom given by

$$B = \frac{mq^4}{2\hbar^2} = 13.6\,\text{eV}, \tag{2.2}$$

a_0 is the Bohr radius given by

$$a_0 = \frac{\hbar^2}{mq^2} = 5.29 \times 10^{-11}\,\text{m} \tag{2.3}$$

and the parameter μ is given by

$$\mu = \left(\frac{\hbar\omega}{B} - 1\right)^{-1/2} \tag{2.4}$$

This equation is valid for $E_\gamma = \hbar\omega \ll mc^2$ and uses the Gaussian unit convention for electromagnetism like the rest of this section.

The assumption that $E_\gamma \ll mc^2$ is valid for our considerations since the redshift for $T = m$ is 2.17×10^9 whereas we are interested in the region of $z \sim 10^3$.

To simplify Equation 2.1, we consider the extremes of μ. In the context of the CMB, the majority of ionising photons we are considering are "low energy"; which is to say, that $E_\gamma \gtrsim B$. From Equation 2.4, we can see that if we make this assumption, $\mu \gg 1$ for photons energies very close to the binding energy of hydrogen. As $\text{arccot}(z) = \arctan(1/z)$ for $z \neq 0$, we can Taylor expand to obtain $\text{arccot}(\mu) = (1/\mu) - \mathcal{O}((1/\mu)^3)$ for large μ.

Therefore the final term on the RHS becomes

$$\frac{\exp(-4\mu\,\text{arccot}\mu)}{1 - \exp(-2\pi\mu)} \approx \exp(-4) \tag{2.5}$$

We can also approximate $(B/\hbar c) \approx 1$ for sufficiently low energy ionising photons in our large μ limit.

After these approximations, we can write the bound-free cross-section as

$$\sigma_{bf} = \frac{2^9\pi^2}{3e^4}\frac{q^2a_0^2}{\hbar c} \tag{2.6}$$

Where we see that for sufficiently large μ, σ_{bf} is independent of ω.

In thermal equilibrium, photoionisation rates and recombination rates must be equal. This allows us to define the recombination cross-section in terms of the

photoionisation cross-section

$$p_e^2 g_p g_e \sigma_{rec} = p_\gamma^2 g_p g_e g_\gamma \sigma_{bf} \tag{2.7}$$

where p_i are the momenta of relative motion of species i with respect to the target particles and g_i are the degeneracy factor of species i.

Rearranging Equation 2.7 and substituting for the electron ($p_e = mv$) and photon momenta ($p_\gamma = \hbar\omega/c$) we obtain the relation

$$\sigma_{rec} = \frac{2(\hbar\omega)^2 \sigma_{bf}}{c^2 m^2 v^2} \tag{2.8}$$

In this recombination process, we can equate the energy of the released photon to the difference in energies of the final and initial state:

$$\hbar\omega = E_\infty - E_0 = \frac{\hbar k^2}{2m} + \frac{q^2}{2a_0} \tag{2.9}$$

where the first term in the RHS is the energy of a free electron of wavenumber k and the second term is the potential energy of a ground state electron in a hydrogen atom (B).

Like with the photoionisation calculation, we can make the reasonable approximation that $T \ll B$ which again is valid within the context of the time around the formation of the CMB. Therefore, the first term can be ignored and we find that $\hbar\omega \approx B$.

For these low energy photons, we can use the large μ limit to find the photoionisation cross-section to be Equation 2.6. Substituting this and equation 2.9 into Equation 2.8 gives

$$\sigma_{rec} = \left(\frac{2^{10}\pi^2}{3e^4}\right) \frac{q^2}{\hbar c} \left(\frac{a_0 B}{mcv}\right)^2 \tag{2.10}$$

From Wascko (2021), the reaction rate per unit volume of a given reaction is

$$R = \phi n \sigma \tag{2.11}$$

where ϕ is the flux of incident particles and n is the number density of the target. Considering this in terms of ground state hydrogen recombination, we find that $\phi = v n_e$ where v is the relative velocity of electrons to the protons (target particles).

For a system with a distribution of electron velocities, we can see that the term $v\sigma_{rec}(v)$ provides the dependence on velocity to the rate of recombination. Therefore,

we can define the recombination coefficient

$$\alpha_{rec} = \langle v\sigma_{rec} \rangle \tag{2.12}$$

such that the average rate of change of electron number density due to recombination is $-\alpha_{rec} n_e n_p$ (Padmanabhan 2000).

To find α, we can take the average over the line by using the 1D Maxwell-Boltzmann equation

$$f(v)\mathrm{d}v = \sqrt{\frac{m}{2\pi T}} \exp\left(-\frac{mv^2}{2T}\right) \mathrm{d}v \tag{2.13}$$

which is the distribution of line of sight velocities in thermal equilibrium.

Substituting for the cross-section in Equation 2.12, we obtain

$$\alpha = \frac{\frac{2^{10}\pi^2}{3e^4}\frac{q^2}{\hbar c}\left(\frac{a_o B}{mc}\right)^2 \int_0^\infty \frac{1}{v} f(v)\mathrm{d}v}{\int_0^\infty f(v)\mathrm{d}v} = \frac{2^{10}\pi^2}{3e^4}\frac{q^2}{\hbar c}\left(\frac{a_o B}{mc}\right)^2 \langle v^{-1} \rangle \tag{2.14}$$

In Padmanabhan (2000), we are given that

$$\langle v^{-1} \rangle = \left(\frac{2m}{\pi T}\right)^{1/2} \tag{2.15}$$

and so we can write the recombination coefficient to ground state as

$$\alpha = \frac{2^{10}\pi^2}{3e^4}\frac{q^2}{\hbar c}\left(\frac{a_o B}{mc}\right)^2 \sqrt{\frac{2m}{\pi T}} = \frac{2^{10}\pi^{3/2}}{3e^4}\left(\frac{q^2}{\hbar c}\right)^3 \left(\frac{a_0^3 B}{\hbar}\right)\left(\frac{B}{T}\right)^{1/2} \tag{2.16}$$

where we used Equation 2.2 for the binding energy.

We can compute the numerical values of α to verify our working with Padmanabhan (2000) which gives the ground state recombination coefficient as

$$\alpha = 1.4 \times 10^{-13} \left(\frac{T}{1\,\mathrm{eV}}\right)^{-1/2} \mathrm{cm}^3 \cdot \mathrm{s}^{-1} \tag{2.17}$$

in Gaussian cgs units. The temperature required for this result corresponds to $1.16 \times 10^4\,\mathrm{K}$ or $1.6022 \times 10^{-12}\,\mathrm{erg}$.

We can substitute the relevant constants in Gaussian units as given in Table 2.1 to Equation 2.16. This gives

$$\alpha = 1.525 \times 10^{-13} \left(\frac{T}{1\,\mathrm{eV}}\right)^{-1/2} \mathrm{cm}^3 \cdot \mathrm{s}^{-1} \tag{2.18}$$

The resulting discrepancy of 8.9% is likely due to the different levels of precision of constants used in the calculation.

Table 2.1: Key constants in SI and Gaussian units from gau (2022).

Constants	Symbol	SI Units	Gaussian CGS Units
electron charge	q	$1.6 \times 10^{-19}\,\mathrm{C}$	$4.8032 \times 10^{-10}\,\mathrm{esu}$
electron mass	m	$9.1095 \times 10^{-31}\,\mathrm{kg}$	$9.1095 \times 10^{-28}\,\mathrm{g}$
speed of light	c	$2.9979 \times 10^{8}\,\mathrm{m \cdot s^{-1}}$	$2.9979 \times 10^{10}\,\mathrm{cm \cdot s^{-1}}$
Boltzmann constant	k_B	$1.3803 \times 10^{-23}\,\mathrm{J \cdot K^{-1}}$	$1.3803 \times 10^{-16}\,\mathrm{erg \cdot K^{-1}}$
reduced Planck constant	$\hbar$	$1.0546 \times 10^{-34}\,\mathrm{J \cdot s}$	$1.0546 \times 10^{-27}\,\mathrm{erg \cdot s}$

We can compare this result with the accepted recombination rate coefficient from cal (2011). In this, we are given that $\alpha = 4.2 \times 10^{-13}\,\mathrm{cm^3 \cdot s^{-1}}$ at $T = 1 \times 10^4\,\mathrm{K}$ and evolves as $\propto T^{-0.7}$ at low temperatures. This significant discrepancy is highlighted in Figure 2.1.

This is clearly beyond error due to using different values of constants especially as the coefficient evolves differently with temperature.

The reason for this discrepancy is due to the fact that our analysis only takes into account recombination directly to ground-state only. To verify that this indeed is causing this discrepancy, we must consider recombination to higher energy levels.

In cal (2011), we are given that the sum of recombination rates from $n = 2$ to ∞ (case B recombination) is equal to $2.6 \times 10^{-13}\,\mathrm{cm^3 \cdot s^{-1}}$ at $T = 10^4\,\mathrm{K}$. Combining this result with Equation 2.18 shows that at first sight, this resolves the discrepancy at $T = 10^4\,\mathrm{K}$.

For more detailed analysis, we must consider the generalisation to Equation 2.7 for recombination to $\mathrm{n^{th}}$ states.

Following the analysis in Section 2.3 to find the recombination coefficients to excited states, we can derive the rate coefficient for recombination from the $\mathrm{n^{th}}$ state to infinity as

$$\alpha(n) = \sum_{i=n}^{\infty} \alpha_i \approx \left(\frac{\sigma_0 c}{2\sqrt{\pi}}\right)\left(\frac{q^2}{\hbar c}\right)^3 \left\{x_n^{3/2} e^{x_n} E_1(x_n) + x_1^{1/2}\left[e^{x_n} E_1(x_n) + \ln x_n + \gamma\right]\right\} \tag{2.19}$$

where $x_n = B/(n^2 T)$ and α_n are the $\mathrm{n^{th}}$ level binding energy to temperature ratio and the rate coefficients to the $\mathrm{n^{th}}$ state respectively. We can use this approximation for ground states to find

$$\alpha_A = \left(\frac{\sigma_0 c}{2\sqrt{\pi}}\right)\left(\frac{q^2}{\hbar c}\right)^3 x_1^{1/2}\left[(x_1+1)e^{x_1} E_1(x_1) + \ln x_1 + \gamma\right] \tag{2.20}$$

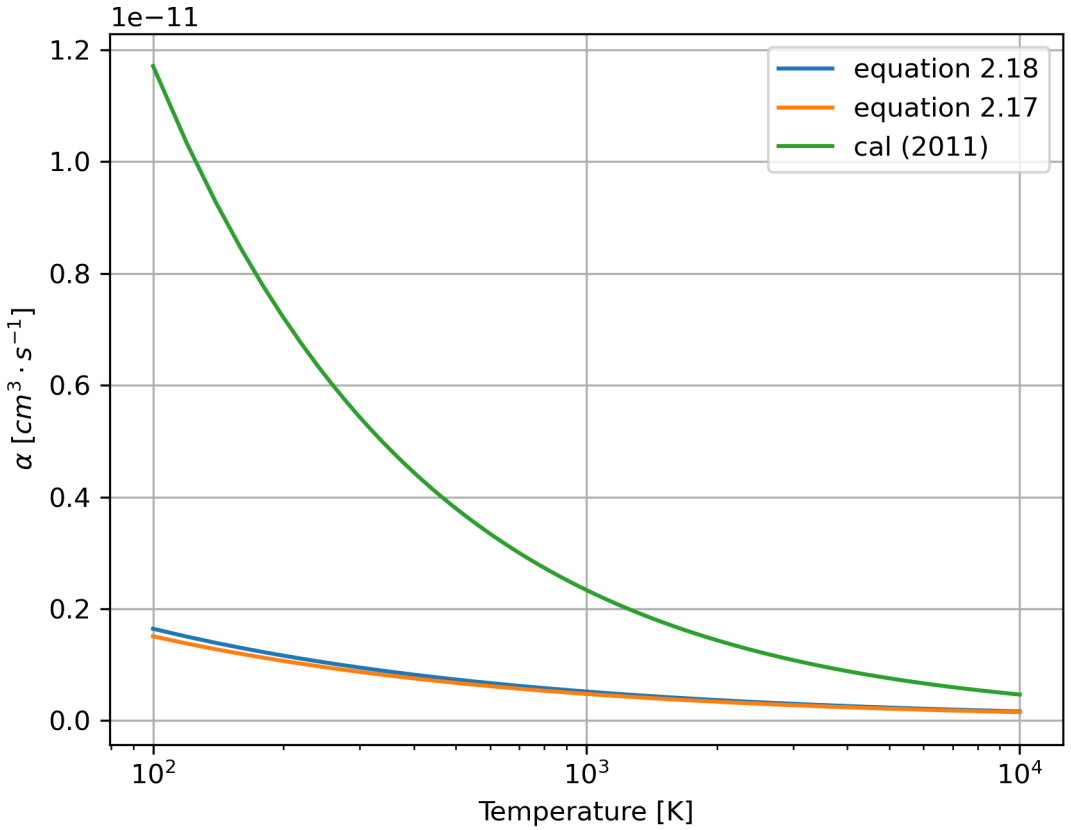

Figure 2.1: plot of Equations 2.17, 2.18 and α_A from cal (2011) over a range of temperatures. We can see that the discrepancy becomes increasingly more significant at lower z.

The temperature dependence of this equation compared to other equations is shown in Figure 2.2 which shows that this equation is well approximated by $\propto T^{-0.7}$ suggested in cal (2011). The discrepancy between the two temperature dependence factors is 3% at $T = 10^3\,\mathrm{K}$.

In fact, when we fit for Equation 2.20 in the same form as cal (2011), we obtain

$$\alpha_A = 3.32 \times 10^{-13} \left(\frac{T}{1\,\mathrm{eV}} \right)^{-0.67} \mathrm{cm}^3 \cdot \mathrm{s}^{-1} \tag{2.21}$$

which has $< 1\%$ discrepancy with Equation 2.20 in the region of $800 < z < 1300$.

Therefore, we have clarified that Equation 2.16 is the rate coefficient for recombination solely to ground state and the total hydrogen recombination coefficient (recombination type A) is given by Equation 2.20 which can be approximated to good accuracy by Equation 2.21.

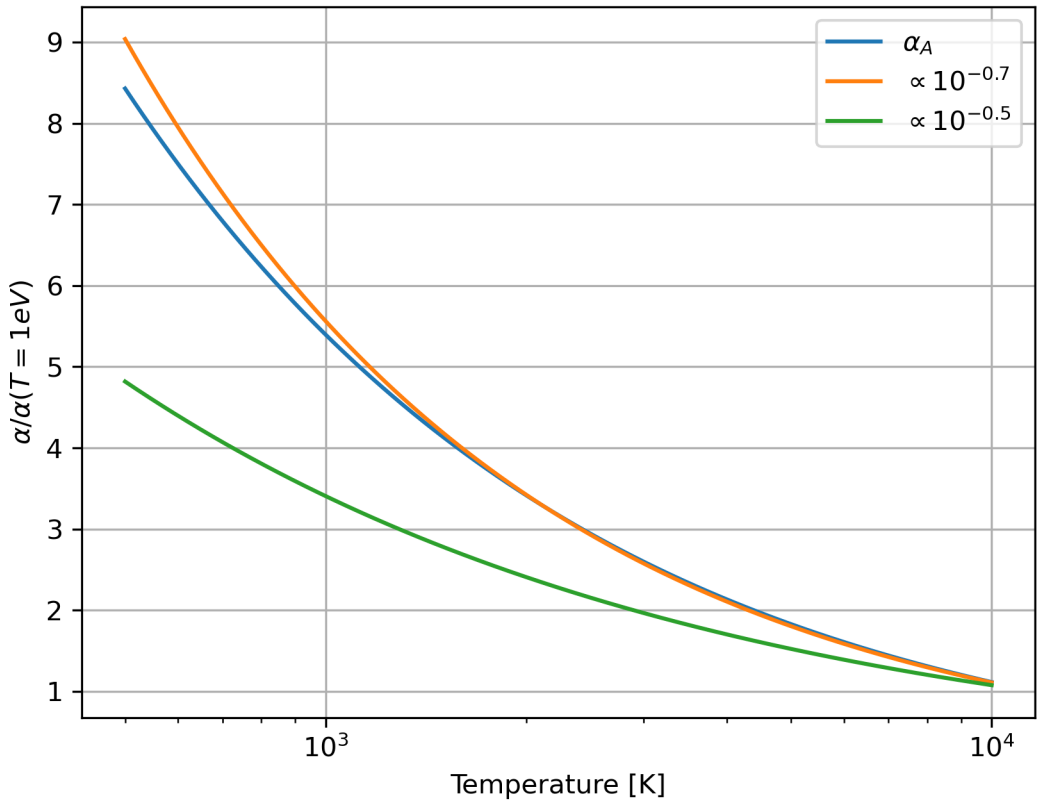

Figure 2.2: The temperature dependence of α for Equations 2.18, from cal (2011) and 2.20. This removes error due to variable choice and shows that the $\propto T^{-0.7}$ is a fit of the full recombination coefficient.

2.2 Saha's Equation

The first step in the formation of the CMB is the sudden increase in neutral matter due to hydrogen recombination (described by Equation 1.16 and rates calculated in Section 2.1) before freezing out.

The matter content just before this point can be considered to be largely ionised (free protons and electrons) and with an initially negligible but increasing fraction of neutral hydrogen.

This matter was in thermodynamic equilibrium with radiation via electron-photon interactions (Compton scattering, free-free absorption and Thomson scattering (Padmanabhan 2002)). These photons can be modelled as a blackbody and their physical number density by

$$n_\gamma(T) = \int_0^\infty \frac{8\pi}{c^3} \frac{\nu^2}{e^{h\nu/T} - 1} = \left(\frac{T}{hc}\right)^3 16\pi\zeta(3) \tag{2.22}$$

(Pritchard 2016) where $\zeta(3)$ is the Riemann zeta function of order 3. By substituting the current temperature of the CMB from Table 1.3, we can find the current CMB photon number density to be $4.09 \times 10^8\,\mathrm{m}^{-3}$ or $409\,\mathrm{cm}^{-3}$ in cgs units.

We can obtain an equation in terms of the redshift by substituting Equation 1.15 where $T \propto (1+z)$.

We can also define the baryon to photon ratio in Table 1.3 in the universe to be

$$\eta = \frac{n_b}{n_\gamma} = 6.05 \times 10^{-10} \tag{2.23}$$

which is a largely invariant quantity from the end of baryogenesis.

From Equation 2.23, we can infer that the current baryonic matter number density in the universe is $0.247\,\mathrm{m}^{-3}$. Using Equation 2.22 and the baryon to photon ratio, we can also extrapolate the baryonic number density to the relevant time period.

We can assume that all relevant particles are in thermal equilibrium with one another. Therefore, we can describe their properties in terms of the temperature ($T(z)$). For the non-relativistic massive particles (e^-, p^+, H), their number density is the Maxwell-Boltzmann distribution given by

$$n_i = g_i \left(\frac{m_i T_i}{2\pi\hbar^2}\right)^{3/2} \exp\left(\frac{\mu_i - m_i}{T_i}\right) \tag{2.24}$$

for species i where g_i and μ_i are the degeneracy factor and the chemical potential of i respectively (Pritchard 2016).

We can make the approximation that $m_p \sim m_H$ and noting that $\mu_e + \mu_p = \mu_H$ and $m_e + m_p - m_H = B$, we can form the Saha equation

$$\frac{n_e n_p}{n_H} = m_e^{3/2} \left(\frac{T}{2\pi\hbar^2}\right)^{3/2} \exp\left(-\frac{B}{T}\right) \tag{2.25}$$

for a system undergoing hydrogen recombination to ground state.

We can now define the ionisation fraction $X = n_p/n_b$ where we know $n_p = n_e$ from the conservation of charge and $n_b = n_p + n_H$ from the conservation of baryon number. Substituting this into Equation 2.25 shows that the left hand side (LHS) is equal to $n_b X^2/(1-X)$ and using Equations 2.23 and 2.22 to express the baryonic number density, we can obtain the equation

$$\frac{1-X}{X^2} = \frac{2^{5/2}}{\sqrt{\pi}} \left(\frac{T}{m_e}\right)^{3/2} \eta\zeta(3) \exp\left(\frac{B}{T}\right) = S(T) \tag{2.26}$$

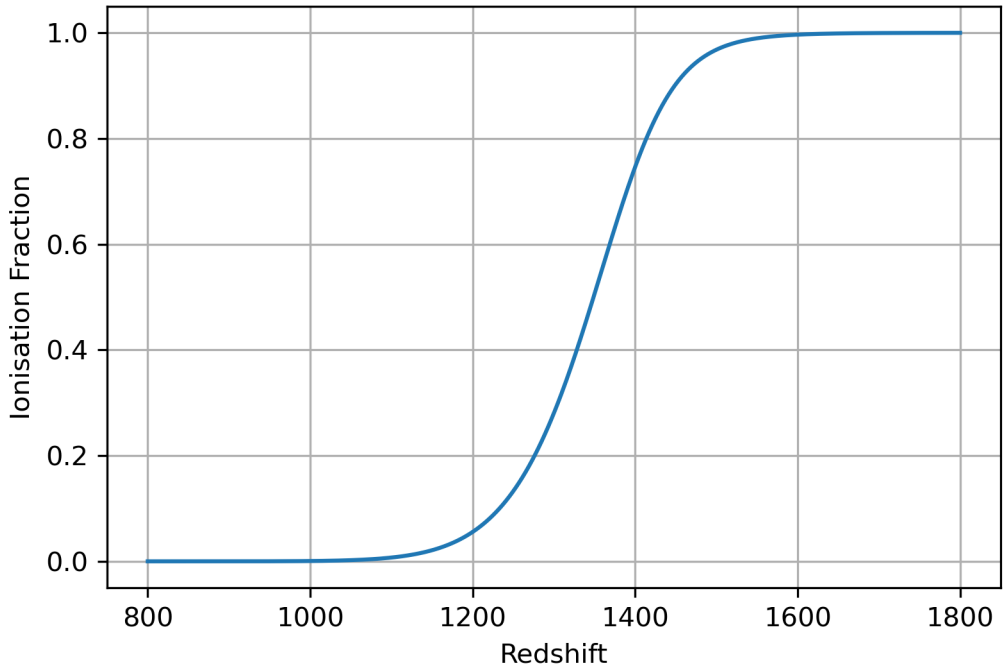

Figure 2.3: Evolution of the ionisation fraction with redshift under equilibrium conditions due to recombination of hydrogen (to ground state) given by Equation 1.16.

This is a simple quadratic in X for which the positive solution will give the ionisation fraction of hydrogen as a function of temperature which can be expressed as a function of redshift using Equation 1.15.

$X \sim 1$ implies that the matter is mostly ionised which is the case for large T (or z). As the universe cools, one can see from Figure 2.3 that there is a sudden shift in X with it falling below half at around $z = 1377$ and almost completely neutral by $z \sim 1100$.

The ionisation fraction will continue to fall with time until the expansion timescale of the universe (H) becomes greater than the recombination rates.

To find when the recombination froze out, we can consider the rate of recombination (Γ) given by the equation

$$\Gamma = n_p \langle \sigma v \rangle = X \eta n_\gamma \alpha \tag{2.27}$$

where α is the recombination rate coefficient defined in Section 2.1 and we have used the definition of the ionisation fraction and the baryon to photon ratio.

Using the ground state recombination rate given by Equation 2.16 we can find the rate of recombination which is displayed on Figure 2.4. The two rates are equal

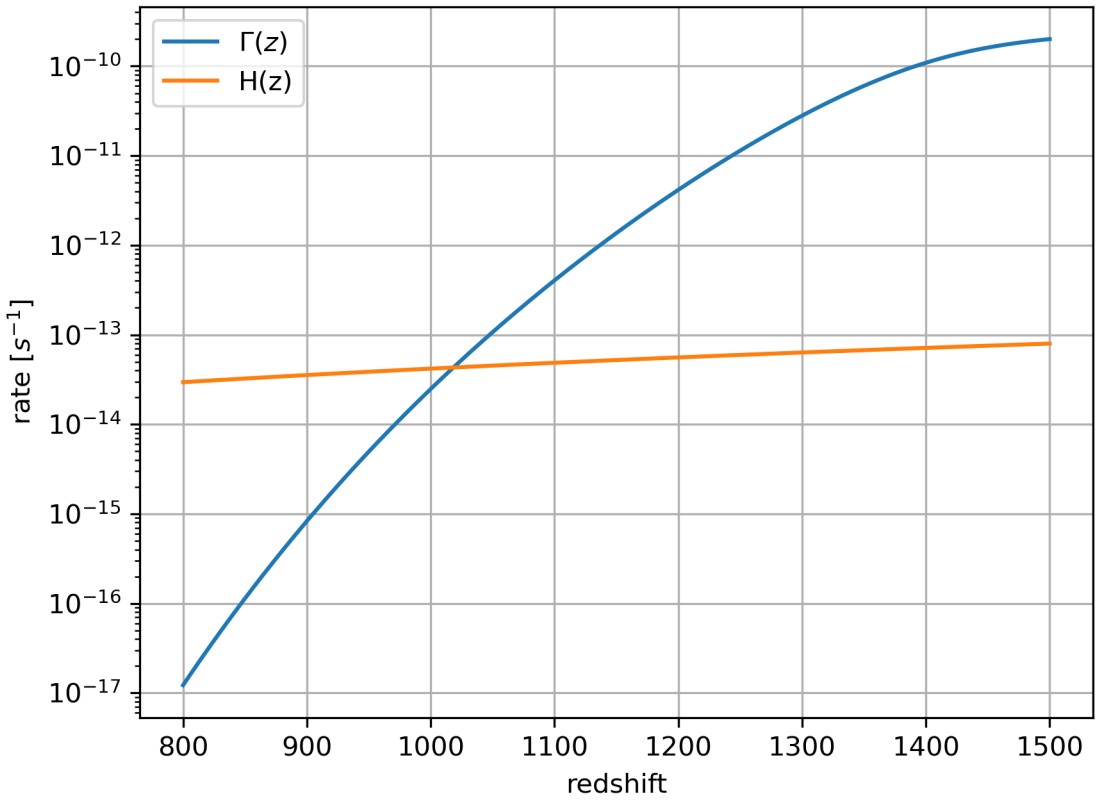

Figure 2.4: plot of recombination rates to ground state and the Hubble parameter.

at $z = 1018$ which gives the remaining free electron fraction as $X(z = 1018) = 5.27 \times 10^{-4}$.

We can now check if this residual electron fraction is sufficient for sustaining matter radiation equilibrium.

The cross-section of Thomson scattering is given by (Pritchard 2016)

$$\sigma_{Th} = \frac{8\pi}{3}\left(\frac{q^2}{mc^2}\right)^2 \tag{2.28}$$

therefore the rate of interaction of photons with free electrons by Thomson scattering is

$$\Gamma_{Th} = X\eta n_\gamma \sigma_{Th} c \tag{2.29}$$

Substituting the values at hydrogen freeze-out, we find that the scattering rate is $2.75 \times 10^{-15}\,\mathrm{s}^{-1}$ which is over an order of magnitude smaller than the Hubble parameter at corresponding z ($4.31 \times 10^{-14}\,\mathrm{s}^{-1}$).

The fact that the lowest energy interaction between free electrons and photons is not feasible at this redshift shows that the photons on average are no longer interacting with matter and therefore the universe is transparent to these photons at this point.

More precisely, the redshift at which Thomson scattering rates equal the expansion rate is at $z = 1124$. We can see that the matter radiation decoupling appears to actually occur just before the recombination freeze-out according to these calculations.

While this is a reasonable starting point, Padmanabhan (2006) notes that this model of the formation of the CMB may not be an accurate description of the model.

In particular, it notes that at $z \approx 10^3$, the effective temperature of the photon blackbody distribution is much less than the binding energy of ground state hydrogen (as we have also seen in the simplifications used in Section 2.1) and therefore, the addition of ionising photons into the system will have a significant affect in the position of the recombination equilibrium. Therefore, it is likely that any recombination directly to ground state (resulting in the emission of an ionising photon) will not affect the net change in ionisation fraction of hydrogen as it will immediately ionise a neighbouring neutral hydrogen as the equilibrium will shift towards the reverse reaction to counteract the change in the system.

Therefore, we would expect the true last scattering surface of photons to occur later on (lower redshift). To find a more accurate model of the ionisation fraction, we must consider the indirect rates of recombination to ground states and recombination to excited states.

2.3 Rate of Recombination to Excited States

In Section 2.1, we discussed the rate of recombination directly to ground state and obtained the equation

$$\alpha_1 = \frac{2^{10}\pi^{3/2}}{3e^4}\left(\frac{q^2}{\hbar c}\right)^3\left(\frac{a_0 B}{\hbar}\right)\left(\frac{B}{T}\right)^{1/2} \tag{2.30}$$

and noted how as this only accounts for the recombination to $n = 1$, we require a generalised recombination coefficient to the n^{th} state.

Padmanabhan (2000) evaluates Equation 2.7 as a function of n and finds the recombination coefficient defined by Equation 2.12. This is given as

$$\alpha_n = \left(\frac{\sigma_0 c}{\sqrt{\pi}}\right)\left(\frac{q^2}{\hbar c}\right)^3 x_n^{3/2} e^{x_n} E_1(x_n) \tag{2.31}$$

where

$$\sigma_0 = \frac{2^6}{3\sqrt{3}}\left(\frac{q^2}{\hbar c}\right)\pi a_0^2 \tag{2.32}$$

is the cross-section of photoionisation from ground state which we found in Section 2.1 in the large μ limit in Equation 2.6. These two terms differ by

$$\sigma_0 = \frac{e^4}{2^3\sqrt{3}\pi}\sigma_{bf}(n=1) = 1.25\sigma_{bf}(n=1), \tag{2.33}$$

$$x_n = \frac{B}{n^2 T} \tag{2.34}$$

is the ratio between the n$^{\text{th}}$ level binding energy ($B_n = B/n^2$) and the thermal energy of the system under thermal equilibrium

and

$$E_1(x) = \int_x^\infty \frac{e^{-u}}{u}\mathrm{d}u = -\gamma - \ln x - \sum_{k=1}^{\infty}\frac{(-x)^k}{kk!} \tag{2.35}$$

is the exponential integral defined in Arfken and Weber (2005) where $\gamma = 0.577$ is the Euler's constant.

Before we proceed with Equation 2.31, we must verify that it is true by comparing to Equation 2.30.

In Section 2.1, we derived Equation 2.30 in the case where $T \ll B$ and therefore $B/T \gg 1$.

In this large x limit, we can use the divergent series for the exponential integral to write

$$e^x E_1(x) = \sum_{n=0}^{\infty}(-1)^n\frac{n!}{x^{n+1}} \tag{2.36}$$

(Arfken and Weber 2005).

We can use this result to linear order on Equation 2.31 for $n = 1$ to find that

$$\alpha(n=1) = \frac{e^4}{2^3\sqrt{3}\pi}\alpha_1 \tag{2.37}$$

where $\alpha(n=1)$ is the Equation 2.31 for $n = 1$. We see that the difference in the two rate coefficients is due to the difference in the calculated ground state photoionisation

cross-section.

In this dissertation, we will use the photoionisation cross-section derived in Section 2.1 which is

$$\sigma_0 = \frac{2^9\pi^2}{3e^4}\frac{q^2a_0^2}{\hbar c} \tag{2.38}$$

In Section 2.2, we noted how direct recombination to ground state does not affect the overall change in electron density of the system. Therefore, to find the effective rate coefficient, we must sum over all n from $n = 2$ to $n = \infty$.

While the higher order terms do decrease in contribution rapidly, it is not the most efficient method to finding α_{ex}. Instead, we can use the trapezoidal rule to approximate

$$\sum_{n=a}^{b} f(n) \approx \frac{f(b) + f(a)}{2} + \int_a^b F(x)\mathrm{d}x \tag{2.39}$$

for summation of integer n with discrete terms represented by function $f(n)$ which are interpolated by the corresponding continuous function $F(x)$. Taking $b \to \infty$ and $a = 2$ for sums of Equation 2.31 gives us

$$\alpha_{\mathrm{ex}} = \left(\frac{\sigma_0 c}{\sqrt{\pi}}\right)\left(\frac{q^2}{\hbar c}\right)^3\left[\frac{1}{2}x_2^{3/2}e^{x_2}E_1(x_2) + \int_2^\infty x_n^{3/2}e^{x_n}E_1(x_n)\mathrm{d}n\right] \tag{2.40}$$

where x_n is defined by Equation 2.34.

To solve the second term on the RHS, we make the substitution,

$$\mathrm{d}n = -x_2^{1/2}\frac{\mathrm{d}x_n}{x_n^{3/2}} \tag{2.41}$$

Therefore the integral becomes

$$Ix_2^{-1/2} = \lim_{a\to 0}\int_a^{x_2} e^x E_1(x)\mathrm{d}x \tag{2.42}$$

where we have moved the $x_2^{1/2}$ to the other side and made the variable change $x_n \to x$ for convenience.

Integrating by parts gives

$$I = \lim_{a\to 0}\left\{[e^x E_1(x)]_a^{x_2} + \int_a^{x_2}\frac{\mathrm{d}x}{x}\right\} \tag{2.43}$$

where we have used the fundamental theorem of calculus and the definition of the exponential integral (Equation 2.35) to obtain the result: $\mathrm{d}[E_1(x)]/\mathrm{d}x = -e^{-x}/x$.

Evaluating Equation 2.43 gives

$$I = e^{x_2} E_1(x_2) + \ln x_2 + \lim_{a \to 0} \left[e^a \left(\gamma + \ln a + \sum_{k=1}^{\infty} \frac{(-x)^k}{k k!} \right) - \ln a \right] \tag{2.44}$$

using Equation 2.35.

Finally, we can make the approximation $e^a \approx 1$ for small a to get

$$a_{\text{ex}} = \left(\frac{\sigma_0 c}{\sqrt{\pi}} \right) \left(\frac{q^2}{\hbar c} \right)^3 x_2^{1/2} \left[x_2 e^{x_2} E_1(x_2) \left(\frac{1}{2} + \frac{1}{x_2} \right) + \gamma + \ln x_2 \right] \tag{2.45}$$

This approximation gives the coefficient of recombination to be $1.86 \times 10^{-13}\,\text{cm}^3 \cdot \text{s}^{-1}$ when $T = 1\,\text{eV}$.

In the case of $x_2 \gg 1$ we can again use the large x limit for the exponential integral given in Equation 2.36 to simplify Equation 2.45 such that

$$\alpha_{\text{ex}} \approx A x_2^{1/2} (x^{-1} + \ln x_2 + 1/2 + \gamma) \tag{2.46}$$

where $A = (\sigma_0 c/\sqrt{\pi})(q^2/\hbar c)^3$.

Then, assuming x_2 is sufficiently large for $1/x_2 \to 0$ and making the approximation that $0.5 + \gamma \sim \ln 4$, we get

$$\alpha_{\text{ex}} \approx \frac{A}{2} \left(\frac{B}{T} \right)^{1/2} \ln \left(\frac{B}{T} \right) \tag{2.47}$$

which is the coefficient of recombination used in Padmanabhan (2006) provided $A/2 = 9.78 r_0^2 c$. Substituting the relevant values, we find them to have a discrepancy of 11%.

In Padmanabhan (2002), we are given an alternative form of the coefficient

$$2.6 \times 10^{-13} T^{-0.8}\,\text{cm}^3 \cdot \text{s}^{-1} \tag{2.48}$$

Where T is the temperature in eV. This is likely to be from a numerical fit for Equation 2.45 over some range of temperatures.

Finally, we can consider the bounds of the infinite sum of coefficients by using the result

$$\int_{n+1}^{\infty} f(x)\mathrm{d}x \leq \sum_{i=n+1}^{\infty} a_i \leq \int_{n}^{\infty} f(x)\mathrm{d}x \tag{2.49}$$

(Palmer 1998) for a converging series if $a_i > 0$ and $f(x = i) = a_i \; \forall i$.

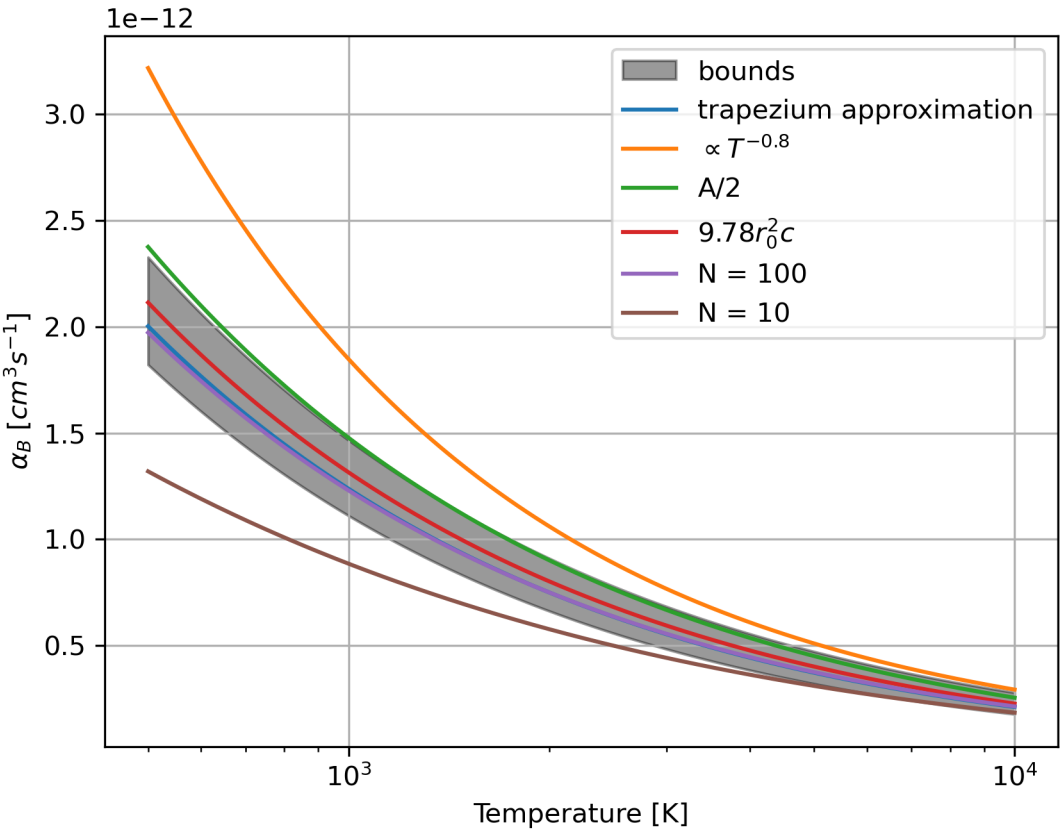

Figure 2.5: The different forms of α_{ex} and the bounds. The N terms indicate the index at which the sum was truncated.

Following the same procedure as the derivation of Equation 2.45, we can compute the integrals for $n = 1$ and compare the different forms of the coefficient in Figure 2.5 along with values of the truncated sum of Equation 2.31.

The graph shows that the trapezium approximation is a good fit against the sum truncated to $N = 100$. It also shows that Equation 2.48 is perhaps not the best approximation to use, given that it is significantly larger (49% discrepancy with the trapezium approximation) although some of this may be due to the term at $T = 1\,\text{eV}$ being greater than the other approximation schemes due to the difference in the precision of the constants used in the derivation. This is highlighted in the discrepancy between the graph of Equation 2.47 using $A/2$ and $9.78 r_0^2 c$ as a prefactor.

We can verify if this is the case by numerically fitting Equation 2.45 over some range of temperature in the same form as Equation 2.48 and the resulting parameters are shown on Table 2.2.

Two different ranges of temperatures were used in fitting as Padmanabhan (2002)

Table 2.2: Fit parameters for both the trapezium approximation and a truncated summation to 1000 terms.

Number of terms	Range of Temperature [K]	Coefficient $[10^{-13}\,\mathrm{cm}^3 \cdot \mathrm{s}^{-1}]$	Exponent
Trapezium	$[800, 1400]$	2.174	-0.709
Trapezium	$[500, 10000]$	2.003	-0.740
$N = 1000$	$[800, 1400]$	2.204	-0.707
$N = 1000$	$[500, 10000]$	2.035	-0.738

does not state the range of temperatures used in the fit. The smaller range is intended to cover the range over which phenomena related to recombination and decoupling occur. I also chose to include the truncated sum in the case that the trapezium approximation deviates from the real α.

The exponent parameters seem to indicate that it may be more than simply differences due to the choice of constants used and therefore, it may be well advised to not use Equation 2.48 until the discrepancy can be further explained.

2.4 Recombination to Excited States

Now with the knowledge of the rates of recombination to excited states, we can attempt to derive how the hydrogen ionisation fraction evolves with time.

In Padmanabhan (2006) this evolution equation is given as

$$\frac{\mathrm{d}X}{\mathrm{d}t} = \alpha \left(\frac{\beta}{\alpha}(1 - X) - n_b X^2 \right) \tag{2.50}$$

where α is the coefficient of recombination given in Equation 2.47 and β is the rate of photoionisation which can be derived by considering the case of thermal equilibrium (ionisation rates = recombination rates) at which we can use the ionisation fraction given by the Saha equation such that

$$\frac{\beta}{\alpha} = \frac{n_\gamma \eta X^2}{1 - X} = \frac{n_\gamma \eta}{S(T)} = \left(\frac{mT}{2\pi\hbar^2} \right)^{3/2} \exp\left(-\frac{B}{T} \right) \tag{2.51}$$

where $S(T)$ is from Equation 2.26. This differs with Padmanabhan (2006) by a factor of $\hbar^{-3}$ which implies the use of natural units in Padmanabhan (2006).

We are then able to make the substitution of

$$\mathrm{d}t = -\frac{\mathrm{d}z}{(1 + z)H_0 E(z)} \tag{2.52}$$

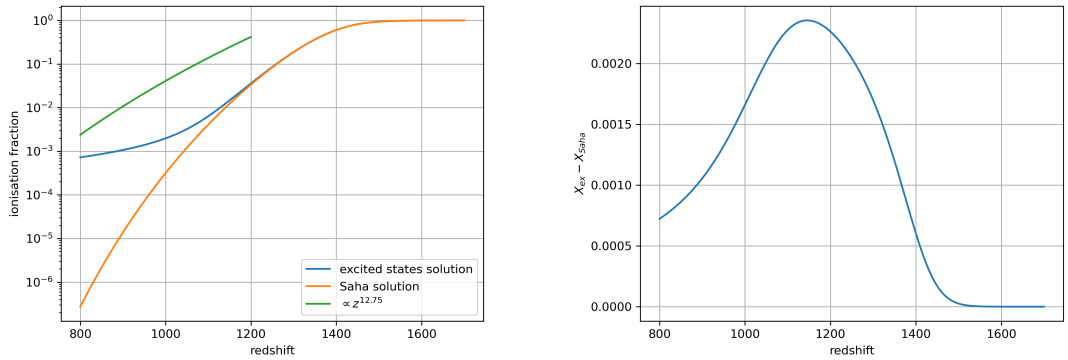

(a) Logarithmic plots of the different ionisation fraction evolution equations. Equation 2.53 was only graphed within the valid range.

(b) Plot of the difference in ionisation fraction between neutral and excited state recombination.

Figure 2.6: Plots of ionisation fractions

Which comes from the definition of the Hubble parameter $H = \dot{a}/a = H_0 E(z)$ and the definition of the cosmological redshift as $(1 + z) = a_0/a$.

In this substitution, we must consider the signs carefully. The ionisation fraction decreases with time and so when evaluated against redshift, we see that it is a positive function. However, as $\mathrm{d}z < 0$, there is an additional negative sign along with the sign from the substitution (although it may be more convenient to evaluate from the upper limit as $X \sim 1$ for sufficiently large z).

In Padmanabhan (2006), a curve fit of the numerical solution valid in the redshift range of $800 < z < 1200$ is given as

$$X = 2.4 \times 10^{-3} \frac{\sqrt{\Omega_m h^2}}{\Omega_b h^2} \left(\frac{z}{1000}\right)^{12.75} \tag{2.53}$$

However, when I numerically integrated Equation 2.50, I found it to be significantly different from Equation 2.53 and visibly almost indistinguishable from the Saha solution from Section 2.2 (Figure 2.3).

Logarithmic scaling of X as shown in Figure 2.6a revealed that there were discrepancies between the Saha solution and the excited state solution. This is more clearly visible on Figure 2.6b were there is a small discrepancy around the range $800 < z < 1200$ as stated in Padmanabhan (2006).

This absolute discrepancy is maximum around $z = 1146$ and at $\Delta(z = 1146) = 2.35 \times 10^{-3}$.

The location of this discrepancy being fairly close to the freeze-out times suggests that this may in fact have some effect on the redshift of freeze-out of recombination

and consequently electron-photon interactions.

From Figure 2.6b, we can also note that the ionisation fraction for excited states is greater than the Saha solution. This implies that the matter remains ionised for longer and so is likely to reach the critical number density for freeze-out and decoupling at a later time. This appears to also agree with what we assumed may happen when not taking into account direct recombination rates to the ground state in Section 2.2.

However, as the fitted solution in Equation 2.53 deviates significantly from both solutions, it may be prudent to consider the evolution of the ionisation fraction in greater detail, particularly as in Padmanabhan (2006), it does not go into how Equation 2.50 is derived.

Padmanabhan (2002) states that the two main routes for the de-excitation to ground state hydrogen from excited states is the two-photon decay from metastable 2S level (rate of $\Lambda = 8.23\,\mathrm{s}^{-1}$) and the resonance transition via the emission of Lyman-α photons.

As the Lyman-α photons are energetic enough to ionise sufficiently excited hydrogen atoms, a net effect of hydrogen formation is only possible with the cosmic redshift of these photons. This effect is given by

$$N_\alpha = e^{-h\nu_\alpha/T} + \frac{c^3}{8\pi\nu_\alpha^3 H} R = e^{-h\nu_\alpha/T} + KR \tag{2.54}$$

where $N_\nu = c^3 n_{nu}/8\pi\nu^2$ is the photon occupation number, ν_α is the mean frequency of Lyman-α photons, R is the rate of formation per unit volume of ground state hydrogen from Lyman-α emission, H is the Hubble parameter, $K = c^3/(8\pi\nu_\alpha^3 H)$ and we have assumed that the photons can be described by a Maxwellian distribution as they are in Equilibrium (Padmanabhan 2002).

We can evaluate the forwards and backwards reactions of the system by using the principle of detailed balance which is given by:

$$g_i C_{ij} e^{-E_i/T} = g_j C_{ji} e^{-E_j/T} \tag{2.55}$$

where C_{ij} and C_{ji} are the forwards and backwards rate coefficients respectively and $g_{i,j}$ and $E_{i,j}$ are the statistical weights and excitation energies (defined as $E_n = B_1 - B_n$ where B is the binding energy of the respective level) of i and j.

We can define β_{ex} as the photoionisation rate (of dimensions of t^{-1}) from excited states and assuming that this process is mainly occurring between free and 2S states,

we have

$$\beta_{\rm ex} e^{-(B_1-B_2)/T} = \alpha_{\rm ex} n_e e^{-B_1/T} \tag{2.56}$$

where n_e is the number density of free electrons given by Equation 2.24. As $m \gg T$, we can approximate $\exp(-m/T) \approx 1$ and therefore,

$$\beta_{\rm ex} = \alpha_{\rm ex} \frac{(2\pi m T)^{3/2}}{h^3} e^{-B_2/T} \tag{2.57}$$

This differs from Equation 2.51 given in Padmanabhan (2006) by $\exp(-1/4)$ coming from the use of different levels of binding energy.

We can also perform a similar analysis on the metastable 2S decay where in equilibrium, we would expect the rate of decay to 1S (Λ) to equal the rate of excitation from 1S to 2S (Λ_{abs}) and so

$$\Lambda e^{-(B_1-B_2)/T} = \Lambda_{abs} e^{-(B_1-B_1)/T} = \Lambda_{abs} \tag{2.58}$$

and therefore, we can write the excitation coefficient in terms of the decay coefficient as $\Lambda_{abs} = \Lambda e^{-h\nu_\alpha/T}$.

If we assume that all the excited hydrogen produced by recombination de-excite to ground state via 2S decay or Lyman-α, we can write the following equation:

$$\alpha_{\rm ex} n_e^2 - \beta_{\rm ex} n_{2s} = R + \Lambda(n_{2s} - n_{1s} e^{-h\nu_\alpha/T}) \tag{2.59}$$

Where n_{1s} and n_{2s} are the number densities of ground state and the $1^{\rm st}$ excited state of hydrogen respectively.

The LHS is the hydrogen recombination rate to excited states per unit volume (recombination - photoionisation rates) and the RHS is the total rate per unit volume of non-direct ground state hydrogen production (Lyman-α + 2S decay - excitation from 1S to 2S).

We can rearrange Equation 2.59 for R which gives

$$R = \alpha_{\rm ex} n_e^2 - \beta_{\rm ex} n_{2s} - \Lambda(n_{2s} - n_{1s} e^{-h\nu_\alpha/T}) \tag{2.60}$$

Substituting this result into Equation 2.54 and using the fact that $N_\alpha = n_{2s}/n_{1s}$ in equilibrium (Padmanabhan 2002) we obtain:

$$N_\alpha = e^{-h\nu_\alpha/T} + K\{\alpha_{\rm ex} n_e^2 - \beta_{\rm ex} n_{1s} N_\alpha - \Lambda n_{1s}(N_\alpha - e^{-h\nu_\alpha/T})\} \tag{2.61}$$

We can rearrange this equation for N_α to get

$$N_\alpha = e^{-h\nu_\alpha/T}\frac{1 + K(\alpha_{\rm ex} n_e^2 e^{h\nu_\alpha/T} + \Lambda n_{1s})}{1 + K n_{1s}(\beta_{\rm ex} + \Lambda)} \tag{2.62}$$

This is different from the equation presented in Padmanabhan (2002) (in the recombination term) but this is likely to be a typo as it leads to the same equation as the book as I will show below.

Now that we have eliminated R and n_{2s} we can attempt to formulate the equation for the evolution of the ionisation fraction ($X = n_e/n_b$).

We know that the LHS of Equation 2.59 is the net recombination rate of hydrogen per unit volume and so must be equal to the loss rate of free electrons in the system so can write:

$$-\frac{{\rm d}n_e}{{\rm d}t} = \alpha_{\rm ex} n_e^2 - \beta_{\rm ex} n_{1s} N_\alpha \tag{2.63}$$

We then substitute in Equation 2.62 for N_α to find

$$-\frac{{\rm d}n_e}{{\rm d}t} = C\left(\alpha_{\rm ex} n_e^2 - \beta_{\rm ex} n_{1s} e^{-h\nu_\alpha/T}\right) \tag{2.64}$$

where

$$C = \frac{1 + K\Lambda n_{1s}}{1 + K n_{1s}(\Lambda + \beta_{\rm ex})} \tag{2.65}$$

To write this equation in terms of X, we can divide through by n_b (baryonic number density) which we can approximate to be equal to the number density of free protons and ground state hydrogen (as we have assumed that all the excited hydrogen formed will de-excite to ground state). Which gives

$$-\frac{\rm d}{{\rm d}t}\left(\frac{n_e}{n_b}\right) = \left(\frac{\alpha_{\rm ex} n_e^2}{n_b} - \frac{\beta_{\rm ex} n_{1s}}{n_b} e^{-h\nu_\alpha/T}\right) C \tag{2.66}$$

As $X = n_e/n_b = n_p/n_b$, Equation 2.66 becomes:

$$-\frac{{\rm d}X}{{\rm d}t} = \{\alpha_{\rm ex} X^2 n_b - \beta_{\rm ex} e^{-h\nu_\alpha/T}(1 - X)\} C(X) \tag{2.67}$$

This is useful as $X = n_e/n_b$ is, as mentioned before, largely invariant against cosmic expansion.

We can also note that Equation 2.67 becomes Equation 2.50 in the case where $C \approx 1$ and $T \gg h\nu_\alpha$. From the latter condition, we can immediately see that this is not likely to be an appropriate simplification given that in our region of interest ($z \sim 10^3$) the opposite is in fact true.

Similarly to Equation 2.50 we can change variables from $t \to z$ using Equation 2.52 to obtain

$$\frac{\mathrm{d}X}{\mathrm{d}z} = \frac{\alpha_{\mathrm{ex}}}{(1+z)H(z)} \left\{ X^2 n_\gamma(z)\eta - \frac{\beta_{\mathrm{ex}}}{\alpha_{\mathrm{ex}}}(z) e^{-h\nu_\alpha/T(z)}(1-X) \right\} C(z) \tag{2.68}$$

where we have made relevant substitutions for z and with $\mathrm{d}z < 0$.

As this equation has multiple parts dependent on z, some of which are rather sensitive to changes in parameters, we can analyse the components of this equation to verify the validity of certain suggested simplifications (like $C \approx 1$) which will also provide greater understanding of the conditions at these times.

2.5 Analysis of the Ionisation Fraction Equation

In the previous section, we derived the equation for the evolution of the ionisation fraction and indicated as to the fact that some of the approximations suggested by Padmanabhan may not be the most appropriate for our relevant region of interest in z.

There are two components of Equation 2.67 which can potentially be simplified: the photoionisation term $I = \beta_{\mathrm{ex}} e^{-h\nu_\alpha/T}(1-X)$ and the "C" term. This section will consider the approximation schemes suggested by Padmanabhan in his derivations for each component and consider their validity within our region of interest.

From Equation 2.50 given in Padmanabhan (2006), we can see by comparing to 2.67, that it approximates that $e^{-h\nu_\alpha/T} \approx 1$ and $C \approx 1$. While in Padmanabhan (2002), it uses $C \approx \Lambda/(\Lambda + \beta_{\mathrm{ex}})$ and $I \approx 0$. The approximations and required conditions for these approximations to hold are summarised below in table 2.3.

Table 2.3: Approximations to Equation 2.67 in Padmanabhan (2006) and Padmanabhan (2002)

Reference	Approximation	Required Conditions
Padmanabhan (2006)	$e^{-h\nu_\alpha/T} \approx 1$	$T \gg h\nu_\alpha$
	$C \approx 1$	$Kn_{1s}(\Lambda + \beta_{\mathrm{ex}}) \ll 1$ or $\beta_{\mathrm{ex}} \ll \Lambda$
Padmanabhan (2002)	$I = \beta_{\mathrm{ex}} e^{-h\nu_\alpha/T}(1-X) \approx 0$	$I \ll \alpha_{\mathrm{ex}} X^2 n_b$
	$C \approx \Lambda/(\Lambda + \beta_{\mathrm{ex}})$	$Kn_{1s}\Lambda \gg 1$

We note that while these approximations are not strictly mutually exclusive, one set of approximations being valid appears to require some fine tuning of other variables in order to satisfy the other set of approximations.

We begin with the temperature condition: an order of magnitude calculation reveals that at $z \sim 10^3$, $h\nu_\alpha/T \approx 50$. Therefore, the complete opposite is in fact

true for the approximation of the distribution of Lyman-α photons. However, this does give weight to the approximation in Padmanabhan (2002) where it assumes that the photoionisation rate is negligible compared to the recombination rate.

Once again using order of magnitude approximations, we find that at $z \sim 10^3$, $\beta_{\text{ex}} \sim 150\,\text{s}^{-1}$ when $\alpha_{\text{ex}} \sim 10^{-12}\,\text{cm}^3 \cdot \text{s}^{-1}$ (from equations for α_{ex} in Section 2.3 evaluated at $z \sim 10^3$). From this, we find that $R_{\text{rec}} = \alpha_{\text{ex}} X^2 n_b \sim 6 \times 10^{-10} X^2\,\text{s}^{-1}$ and $I \sim 1.5 \times 10^{-15}(1 - X)\,\text{s}^{-1}$. So for most values of X, we would indeed expect $R_{\text{rec}} \gg I$ and in fact the rates are equal at around $X \sim 10^{-3}$.

While this is a low number, a slight cause for concern is the fact that in Section 2.2, we found that the residual free electron fraction at recombination freeze-out is 5.27×10^{-4}. However, a more careful calculation reveals that recombination rates $\gg$ photoionisation rates for sufficiently small X and z. This is due to the exponential dependence with temperature for I which ensures that the photoionisation rates remain sufficiently below the recombination rates even at the low levels of residual free electron density.

By definition, the Saha equation models the evolution of the ionisation fraction in the expanding universe for a system in which the forward and backward reactions are in equilibrium. We can see from Figure 2.7 that the net rates largely follow the recombination rates with values of order $10^{-10}\,\text{s}^{-1}$ for trajectories above the Saha line. An example of this is given in the form of the line obtained from the CAMB simulations which considers the excited state recombination rates much like our derivation in Section 2.4.

However, Figure 2.7 also shows that the effects of photoionisation does increase at higher z (again due to the exponential dependence in temperature) and so at sufficiently high z, we may observe some effects of I even at $X \lesssim 1$. Therefore, if we choose to integrate Equation 2.68 over an extended range of z, we may not be able to ignore the photoionisation term and doing so may push the ionisation fraction down at these higher redshifts.

Next, we consider the ratio $\beta_{\text{ex}}/\Lambda$ which is an important condition in C. As $\Lambda = 8.23\,\text{s}^{-1}$ we find this ratio to be an exponentially increasing function in z. Once again using the order of magnitude values, we find this ratio to be ~ 20 at $z \sim 10^3$ which is in rough agreement with the equation given in (Padmanabhan 2002) where we can evaluate the ratio between the terms to be ~ 80 in similar conditions. The ratio reaches unity at around $z \approx 850$ by which we would expect recombination to have already frozen-out and decoupling to have occurred.

The ratio of de-excitation rates to ground state via Lyman-α and 2S-decay of

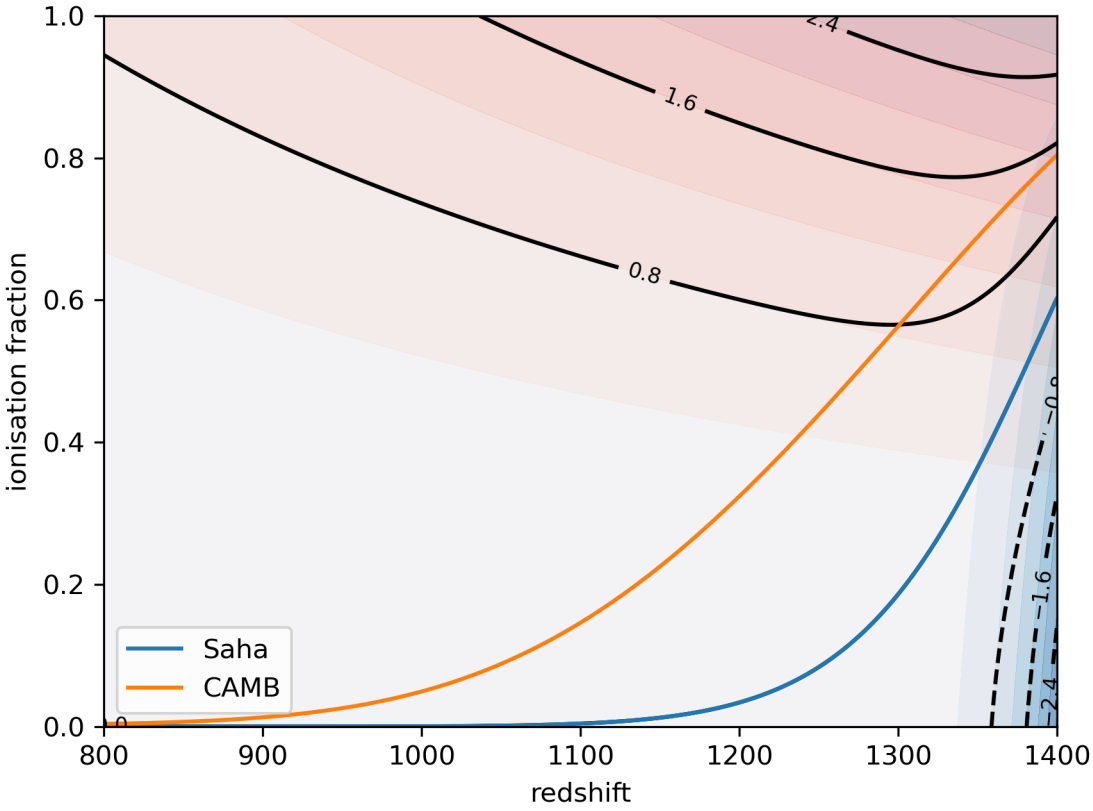

Figure 2.7: The red contours represent the recombination rates, blue represents the photoionisation rates and the black contour lines are the net rates given in units of $10^{-10}\,\mathrm{s}^{-1}$ (solid lines > 0, dotted lines < 0). The trajectory of X is superimposed for both the Saha model and CAMB background model using standard cosmological parameters given in Table 1.3.

hydrogen can be written as:

$$R_{1s} = \frac{R}{\Lambda n_{1s}(N_\alpha - e^{-h\nu_\alpha/T})} = \frac{\alpha_{\mathrm{ex}} n_e^2 - \beta_{\mathrm{ex}} n_{1s} N_\alpha - \Lambda n_{1s}(N_\alpha - e^{-h\nu_\alpha/T})}{\Lambda n_{1s}(N_\alpha - e^{-h\nu_\alpha/T})} \tag{2.69}$$

where we have used Equation 2.60 for R.

We can then substitute Equation 2.62 for N_α which gives

$$\frac{\alpha_{\mathrm{ex}} n_e^2 e^{h\nu_\alpha/T} - \beta_{\mathrm{ex}} n_{1s} D - \Lambda n_{1s}(D-1)}{\Lambda n_{1s}(D-1)} \tag{2.70}$$

where we define D as

$$N_\alpha = e^{-h\nu_\alpha/T} \frac{1 + K(\alpha_{\mathrm{ex}} n_e^2 e^{h\nu_\alpha/T} + \Lambda n_{1s})}{1 + K n_{1s}(\beta_{\mathrm{ex}} + \Lambda)} = e^{-h\nu_\alpha/T} D \tag{2.71}$$

Evaluating the denominator gives

$$\Lambda n_{1s}(D-1) = \Lambda n_{1s} \frac{K(\alpha_{\text{ex}} n_e^2 e^{h\nu_\alpha/T} - n_{1s}\beta_{\text{ex}})}{1 + K n_{1s}(\beta_{\text{ex}} + \Lambda)} \tag{2.72}$$

and the numerator gives

$$\alpha_{\text{ex}} n_e^2 e^{h\nu_\alpha/T} - \beta_{\text{ex}} n_{1s} D - \Lambda n_{1s}(D-1) = \frac{\alpha_{\text{ex}} n_e^2 e^{h\nu_\alpha/T} - \beta_{\text{ex}} n_{1s}}{1 + K n_{1s}(\beta_{\text{ex}} + \Lambda)} \tag{2.73}$$

after a fair bit of algebra.

Equation 2.69 then simply gives

$$R_{1s} = \frac{1}{\Lambda n_{1s} K} = \frac{1}{\Lambda n_\gamma \eta (1-X) K} \tag{2.74}$$

The inverse of this ratio appears in Equation 2.65 for C in both the denominator and the numerator terms. Therefore, understanding how this de-excitation ratio evolves will provide an insight into the state of the universe at the relevant period and whether some of the simplifications carried out in analysis of the ionisation fraction is indeed justified.

For $C \approx \Lambda/(\Lambda + \beta_{\text{ex}})$ to be valid, we would need $R_{1s} \ll 1$ in Equation 2.74 according to conditions given in Table 2.3. Figure 2.8 indicates that for all trajectories following the shape of the Saha curve in this recombination phase, we expect to have a sharp transition in R_{1s} from $\sim \infty$ pre-recombination to $\sim 1/3$ before slowly tending once again to ∞ post-recombination.

From this, we expect $C \approx 1$ to be only valid well past the recombination freeze-out phase given that $\beta_{\text{ex}} \gg \Lambda$ for higher z which prevents C from increasing despite the small R_{1s}. We can also note that $C \approx \Lambda/(\Lambda + \beta_{\text{ex}})$ would only be valid for a short phase in which recombination actively occurs and the accuracy of the approximation even for this region remains questionable given that the maximum $R_{1s}^{-1} \approx 3$.

To know whether $R_{1s}^{-1} \approx 3$ is sufficiently large for this approximation to hold in the key region, we can compute Equation 2.65 for different values of z and X and compare with the values of the approximated C at the relevant redshifts. Figure 2.9a appears to show that we would again need to maintain a high X in order for this approximation to be valid. We expect the curve for C to shift downwards as shown with the decreasing ionisation fraction and therefore would expect the error to increase. This is shown in Figure 2.9b which shows that we have very large fractional errors reaching up to ~ 5 times the true value in C, particularly in the region $800 < z < 1400$ which happens to be the range at which we would expect

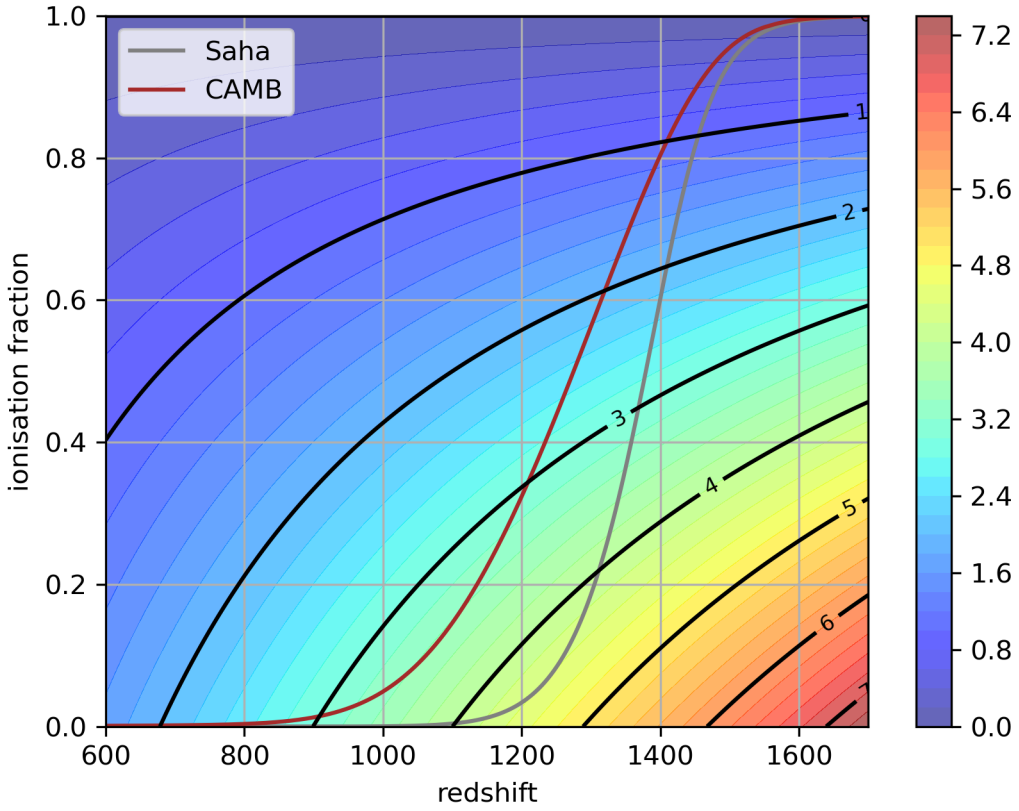

Figure 2.8: Map of $R_{1s}^{-1} = \Lambda n_{1s} K$ superimposed with path of the evolution of X according to Saha and CAMB models.

this recombination rate transition to take place.

The result of this large discrepancy is that the difference in the rate of change of the ionisation fraction in these appropriate redshifts are much greater than the true value of $\mathrm{d}X/\mathrm{d}z$ as shown in Figure 2.10 (the fractional error ranges between $3 \sim 5$ times the relevant true value in the redshift range $800 < z < 1400$).

As shown in Figure 2.9a, the approximation for C does follow the general shape of the actual values of C and as shown above, the photoionisation rates can be considered negligible for lower redshifts. Therefore the approximations used in Padmanabhan (2002) may be used to obtain a general understanding of the evolution of the ionisation fraction within the recombination phase of the universe but the specific values obtained using these calculations may potentially be different from the true value.

To solve Equation 2.68 for X, we can numerically integrate the differential equation. Integrating from pre-recombination is difficult due to the initial value of X as

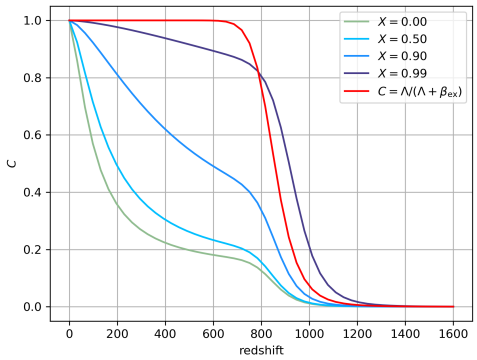

(a) Evolution of C for a range of values of X. The evolution of the universe indicates that C will shift down as z decreases.

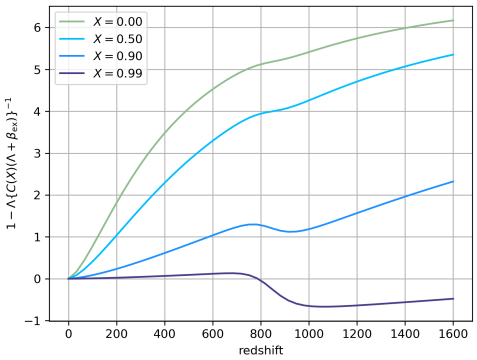

(b) Plot of the fractional error in C of the approximation $\Lambda/(\Lambda + \beta_{\text{ex}})$ for different values of X.

Figure 2.9: Plots to compare the approximation $C \approx \Lambda/(\Lambda + \beta_{\text{ex}})$ to Equation 2.65.

well as its rate of change being very small for low redshifts and therefore, solution becomes extremely sensitive to initial conditions as well as the step size. Instead, we can assume that for the pre-recombination era, at sufficiently high z, the universe is such that the ionisation fraction can be modelled well by the Saha equation (the system is in thermal equilibrium). We can use this initial condition pre-recombination to solve for X.

If we consider the approximations in Table 2.3 made by Padmanabhan (2002), Equation 2.68 becomes

$$\frac{\mathrm{d}X}{\mathrm{d}z} = \frac{\alpha_{\text{ex}}\eta n_\gamma}{(1+z)E(z)(1+\beta_{\text{ex}}/\Lambda)} \tag{2.75}$$

The fractional error of the rate of change of X between Equation 2.75 and 2.68 is shown in Figure 2.10 which shows that the approximated rate of change in X is significantly larger than the actual value. Therefore, we would expect the ionisation fraction of Equation 2.75 to fall faster than the full solution but not as quickly as the Saha equation.

We can solve Equation 2.75 in the same way as equation 2.68 with the same initial conditions. Padmanabhan (2002) also provides us with a suggested fit of the solution valid in the range $800 < z < 1200$ given by

$$X = 2.4 \times 10^{-3} \frac{(\Omega_m h^2)^{1/2}}{\Omega_b h^2} \left(\frac{z}{1000}\right)^{12.75} \tag{2.76}$$

These solutions for X are shown in Figure 2.11. The no photoionisation solution

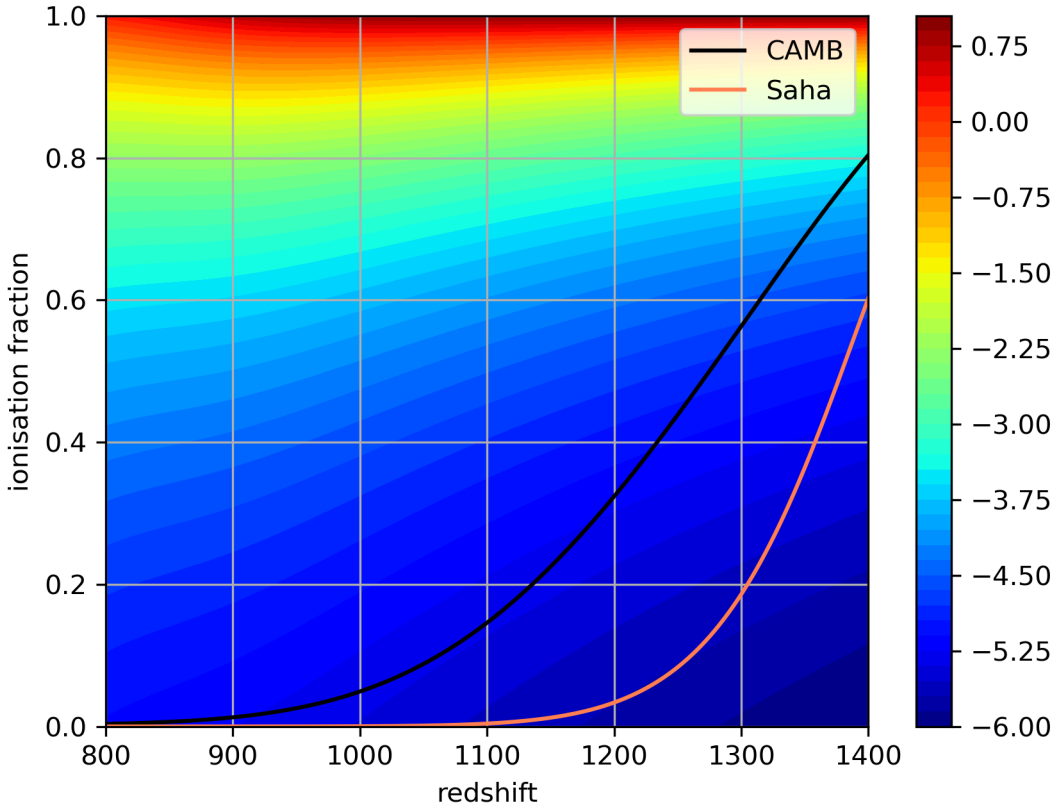

Figure 2.10: Fractional error in $\mathrm{d}X/\mathrm{d}z$ given by the approximate Equation 2.75 and the full Equation 2.68. Saha's solution and CAMB background evolution solution have been included to provide an indication of the trajectory of the evolution.

behaves as we expected by being forced down at higher z due to the lack of photoionisation to increase the ionisation fraction. However, this figure also appears to show that while the CAMB simulated background evolution seems to follow the full solution initially, it quickly proceeds to follow the solution to Equation 2.75, which we showed above was not suitable in approximating for the ionisation fraction within this region.

Figure 2.10 does explain the shape of the Padmanabhan curve in Figure 2.11 as the approximated rate is significantly larger than the true rate and increases relative to the true rate as it approaches $z = 10^3$ before gradually decreasing after recombination. However, it is interesting to note that the CAMB background solution also appears to follow this approximated scheme. The reason behind this may be due to extra physics and interactions I have currently not accounted for which push the ionisation fraction to evolve like Equation 2.75.

As the solution to Equation 2.68 is much greater than the CAMB background

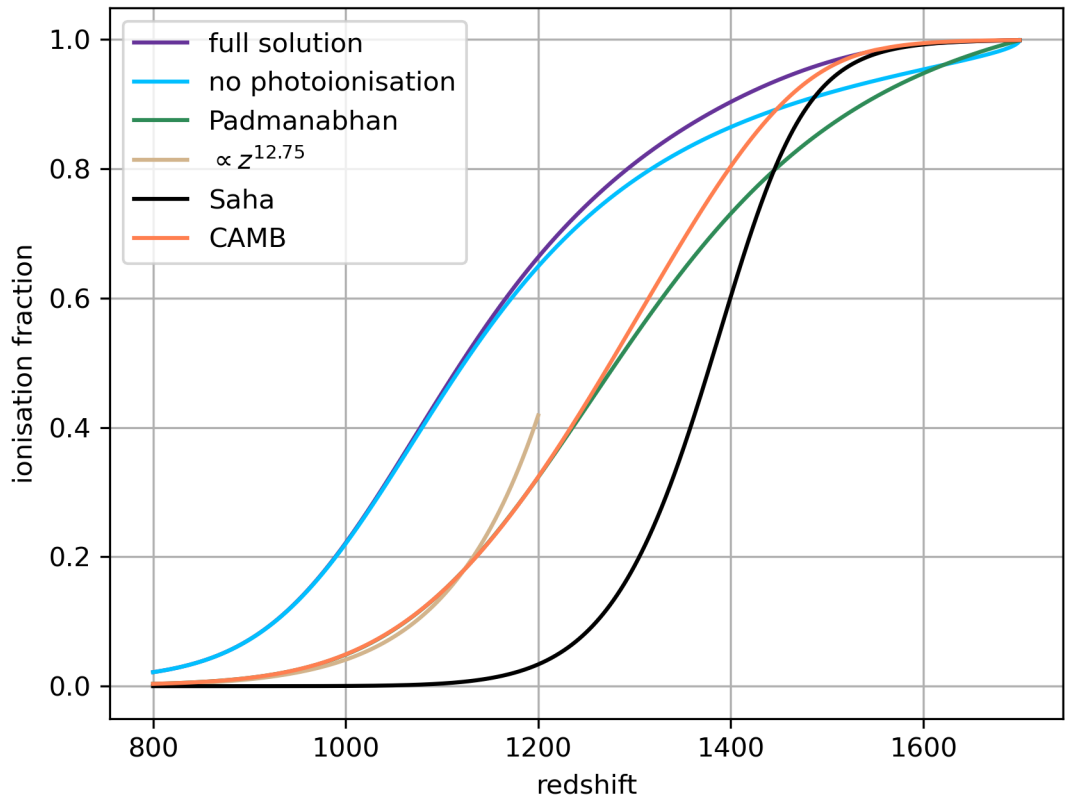

Figure 2.11: Plot of the solutions of X. no photoionisation is the solution which ignores the β_{ex} term in Equation 2.68 and Padmanabhan is the solution to Equation 2.75.

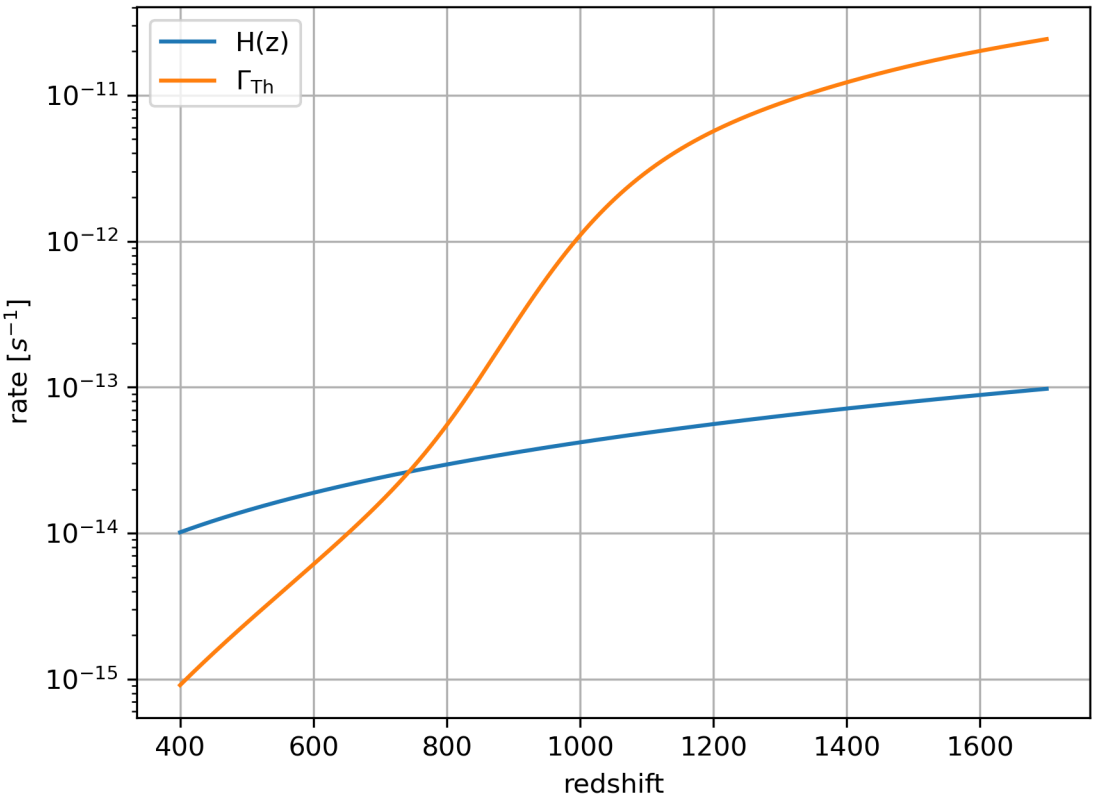

Figure 2.12: Plot of the expansion rate of the universe and the interaction rate of Thomson scattering in a universe where the ionisation fraction evolves according to Equation 2.67.

model at lower z, if we are able to compare it with the measured present-day ionisation fraction in the universe, this will be able to confirm that the derivation used in this dissertation is insufficient in its description of the Hydrogen recombination phase of our universe.

Using the full solution for X in Equation 2.29, we can find the rate of interaction of Thomson scattering if the ionisation fraction in our universe evolved according to Equation 2.67. This interaction rate can be seen in Figure 2.12 and the decoupling occurs at $z = 743.4$.

3 Perturbations in the CMB

3.1 Cosmological Perturbation Theory

While the universe is largely isotropic and homogeneous, we know that there exist perturbations from the background in our universe as of course, we exist. If the perturbations are small, we can introduce a small perturbation to the background and analyse how this evolves at linear order.

For a flat background universe, we can use the FRW metric given in Equation 1.1 to write the metric tensor as

$$\bar{g}_{\mu\nu} = \begin{pmatrix} -1 & \mathbf{0} \\ \mathbf{0} & a^2(t)\delta_{ij} \end{pmatrix} \tag{3.1}$$

where the Greek indices run over the 4D spacetime and the Latin indices run over the spatial coordinates. $\bar{g}_{\mu\nu}$ is the background metric tensor, $a(t)$ is the scale factor as a function of time and δ_{ij} is the Kronecker delta.

We can then introduce conformal time (η not to be confused with the photon to baryon ratio in Table 1.3) defined as

$$\mathrm{d}t = a\mathrm{d}\eta \tag{3.2}$$

which allows us to write the background metric as

$$\mathrm{d}s^2 = a^2(-\mathrm{d}\eta^2 + \mathrm{d}x^2 + \mathrm{d}y^2 + \mathrm{d}z^2) \tag{3.3}$$

and so the background metric tensor becomes

$$\bar{g}_{\mu\nu} = a^2(\eta)\eta_{\mu\nu} \tag{3.4}$$

where $\eta_{\mu\nu}$ is the Minkowski metric.

We can also use Equation 3.2 to write the Friedmann equation (Equation 1.2) as

$$\mathcal{H}^2 = \left(\frac{8\pi G\bar{\rho}}{3}\right) a^2 \tag{3.5}$$

where we have Incorporated Λ into the background density $\bar{\rho}$ by considering its effective density $\bar{\rho}_\Lambda = \Lambda/(8\pi G)$ and we have introduced the conformal Hubble parameter $\mathcal{H}$ which is defined as

$$\mathcal{H} = \frac{a'}{a} \tag{3.6}$$

where

$$' = \frac{\mathrm{d}}{\mathrm{d}\eta} = a\frac{\mathrm{d}}{\mathrm{d}t} \tag{3.7}$$

is the derivative with respect to the conformal time.

The acceleration equation (Equation 1.3) is given by

$$\frac{a''}{a} - \left(\frac{a'}{a}\right)^2 = \frac{4\pi G}{3}(\bar{\rho} + 3\bar{p})a^2 \tag{3.8}$$

where $\bar{p}$ is the background pressure related to the background density by $\bar{p} = w\bar{\rho}$.

Using our definition of the conformal Hubble parameter in Equation 3.6, we can rewrite the equation above as

$$\mathcal{H}' = \frac{4\pi G}{3}(\bar{\rho} + 3\bar{p})a^2 \tag{3.9}$$

Similarly, we can express the energy conservation equation in Equation 1.6 as

$$\bar{\rho}' = -3\mathcal{H}(\bar{\rho} + \bar{p}) \tag{3.10}$$

which allows us to solve for the evolution of the scale factor in matter and radiation dominant phases as a function of η like for Table 1.1, which gives us the results in Table 3.1.

Table 3.1: Solutions for Equation 3.5 for radiation and matter dominated phases. a_0 is the scale factor at present conformal time denoted by η_0.

Phase	w	$a(\eta)$	$\mathcal{H}(\eta)$
Radiation	$\frac{1}{3}$	$a_0\left(\frac{\eta}{\eta_0}\right)$	$\frac{1}{t}$
Matter	0	$a_0\left(\frac{\eta}{\eta_0}\right)^2$	$\frac{2}{t}$

We can write the full perturbed metric tensor in conformal time as a sum of the

background and a small, linear perturbation expressed as

$$g_{\mu\nu} = \bar{g}_{\mu\nu}(\eta) + \delta g_{\mu\nu}(\eta, x^i) \tag{3.11}$$

where the linear perturbation can be a function of all components of spacetime. We note that both the perturbed ($\delta g_{\mu\nu}$) and the background ($\bar{g}_{\mu\nu}$) metric tensors do not live in the perturbed spacetime but can be written in such form.

This perturbation can be written as

$$\delta g_{\mu\nu} = a^2 \begin{pmatrix} -2A & -B_i \\ -B_i & 2C_{ij} \end{pmatrix} \tag{3.12}$$

where A is a scalar function expressing the proper time between hypersurfaces of constant time known as the lapse function, B_i is the spatial vector along a given hypersurface known as the shift vector and C_{ij} is the spatial perturbation (Kurki-Suonio 2022).

So the full perturbed metric tensor in Equation 3.11 can be written as

$$g_{\mu\nu} = a^2 \begin{pmatrix} -(1+2A) & -B_i \\ -B_i & \delta_{ij} + 2C_{ij} \end{pmatrix} \tag{3.13}$$

and its contravariant counterpart can be found using the relation $g_{\mu\lambda}g^{\lambda\nu} = \delta^\nu_\mu$. The background inverse metric is just $\bar{g}^{\mu\nu} = a^{-2}\eta^{\mu\nu}$ and the perturbed metric tensor is

$$g^{\mu\nu} = a^{-2} \begin{pmatrix} -1+2A & -B_i \\ -B_i & \delta_{ij} - 2C_{ij} \end{pmatrix} \tag{3.14}$$

The geometry of spacetime with matter is described by the Einstein equations

$$G_{\mu\nu} = 8\pi G T_{\mu\nu} \tag{3.15}$$

where $G_{\mu\nu}$ is the Einstein tensor and $T_{\mu\nu}$ is the stress-energy tensor using $c = 1$ and ignoring the cosmological constant term $-g_{\mu\nu}\Lambda$. The Einstein tensor describing the curvature of spacetime can be written as

$$G_{\mu\nu} = R_{\mu\nu} - \frac{1}{2} g_{\mu\nu} R^\lambda_\lambda \tag{3.16}$$

which is the trace-reverse of the Ricci tensor ($R_{\mu\nu}$) which in turn can be described

in terms of the Christoffel symbols ($\Gamma^{\alpha}_{\beta\gamma}$) so that

$$R_{\mu\nu} = \Gamma^{\alpha}_{\nu\mu,\alpha} - \Gamma^{\alpha}_{\alpha\mu,\nu} + \Gamma^{\alpha}_{\alpha\beta}\Gamma^{\beta}_{\nu\mu} - \Gamma^{\alpha}_{\nu\beta}\Gamma^{\beta}_{\alpha\mu} \tag{3.17}$$

and finally

$$\Gamma^{\alpha}_{\mu\nu} = \frac{1}{2} g^{\alpha\lambda}(g_{\lambda\mu,\nu} + g_{\lambda\nu,\mu} - g_{\mu\nu,\lambda}) \tag{3.18}$$

The stress-energy tensor is

$$T_{\mu\nu} = (\rho + p)u_{\mu}u_{\nu} + pg_{\mu\nu} + \Pi_{\mu\nu} \tag{3.19}$$

where u_{μ} is the 4-velocity vector defined by

$$\begin{aligned} u^{\mu} &= \frac{\mathrm{d}x^{\mu}}{\mathrm{d}\tau} \\ u_{\mu}u^{\mu} &= g_{\mu\nu}u^{\mu}u^{\nu} = -1 \end{aligned} \tag{3.20}$$

where τ is the proper time and $\Pi_{\mu\nu}$ is the anisotropic stress tensor which satisfies the conditions

$$\begin{aligned} \Pi^{\mu}_{\mu} &= 0 \\ u^{\mu}\Pi_{\mu\nu} &= 0 \end{aligned} \tag{3.21}$$

so that it is a traceless, spatial tensor.

The particles which exist within this spacetime travel along geodesics which are given as

$$\frac{\mathrm{d}^2 x^{\mu}}{\mathrm{d}\lambda^2} + \Gamma^{\mu}_{\alpha\beta}\frac{\mathrm{d}x^{\alpha}}{\mathrm{d}\lambda}\frac{\mathrm{d}x^{\beta}}{\mathrm{d}\lambda} = 0 \tag{3.22}$$

where $\Gamma^{\mu}_{\alpha\beta}$ is the Christoffel symbol defined by Equation 3.18 and λ is an affine parameter of the geodesic.

Like the linearisation of the metric tensor into background and first order perturbations, we can also linearise the Einstein equation such that

$$\begin{aligned} \bar{G}_{\mu\nu} &= 8\pi G\bar{T}_{\mu\nu} \\ \delta G_{\mu\nu} &= 8\pi G\delta T_{\mu\nu} \end{aligned} \tag{3.23}$$

where $G_{\mu\nu} = \bar{G}_{\mu\nu} + \delta G_{\mu\nu}$ and $T_{\mu\nu} = \bar{T}_{\mu\nu} + \delta T_{\mu\nu}$ have been divided into background and perturbation terms. The background spacetime is described by the background metric tensor given in Equation 3.4 describing a flat FRW universe.

In the flat FRW background universe, due to the cosmological principle, pressure and density of matter are solely dependent on time and must be at rest (spatial com-

ponents of the 4-velocity of matter are 0). Therefore, the contravariant background 4-velocity is

$$\bar{u}^\mu = a^{-1}(1, \mathbf{0}) \tag{3.24}$$

as $a^2\eta_{00}(u^0)^2 = -1$ using Equation 3.20 on the background quantities.

We can define the full 4-velocity to be $u^\mu = \bar{u}^\mu + \delta u^\mu = (1/a + \delta u^0, \delta u^i)$. The chronal contravariant component of the perturbation to the 4-velocity can be found by using the perturbed metric in Equation 3.13 to obtain

$$\begin{aligned} g_{\mu\nu}u^\mu u^\nu &= g_{00}u^0u^0 = -1 \\ &= -a^2\left(1+2A\right)\left(\frac{1}{a} + \delta u^0\right)^2 \\ &= -(1 + 2a\delta u^0 + 2A) + \mathcal{O}(\epsilon^2) \end{aligned} \tag{3.25}$$

as the spatial terms of the 4-velocity vector are pure perturbations and so can be ignored when linearising this equation. Rearranging this gives $\delta u^0 = -A/a$.

We can define the 3-velocity perturbation as

$$v_i = au^i \tag{3.26}$$

which allows us to write the 4-velocity of matter in the perturbed universe as

$$u^\mu = \frac{1}{a}\left(1 - A, v_i\right) \tag{3.27}$$

and we can lower the index using our metric tensor from Equation 3.13 to find the covariant velocity 4-vector

$$u_\mu = -a\left(1 + A, B_i - v_i\right) \tag{3.28}$$

to linear order in perturbations.

For a flat FRW universe, we would expect the stress-energy tensor of the matter contents to be a perfect fluid ($\Pi_{\mu\nu} = 0$). Substituting this and the background 4-velocity vector (Equation 3.24) into Equation 3.19 give the background tensor

$$\bar{T}_{\mu\nu} = a^2\begin{pmatrix} \bar{\rho} & \mathbf{0} \\ \mathbf{0} & \bar{p}\delta_{ij} \end{pmatrix} \tag{3.29}$$

where $\bar{\rho}$ and $\bar{p}$ are the background density and pressure respectively. For convenience,

we can raise an index to write

$$\bar{T}^{\mu}_{\nu} = a^{-2}\eta^{\mu\alpha}\bar{T}_{\alpha\nu} = \begin{pmatrix} -\bar{\rho} & \mathbf{0} \\ \mathbf{0} & \bar{p}\delta^{i}_{j} \end{pmatrix} \tag{3.30}$$

where Equation 3.19 now becomes

$$\begin{aligned} T^{\mu}_{\nu} &= g^{\mu\alpha}T_{\alpha\nu} \\ &= (\rho + p)u^{\mu}u_{\nu} + p\delta^{\mu}_{\nu} + \Pi^{\mu}_{\nu} \end{aligned} \tag{3.31}$$

To find the perturbed stress-energy tensor, we can substitute our 4-velocity vectors in Equations 3.27 and 3.28 as well as $\rho = \bar{\rho} + \delta\rho$ and $p = \bar{p} + \delta p$ for the perturbed density and pressure respectively. This gives

$$\begin{aligned} T^{\mu}_{\nu} &= \bar{T}^{\mu}_{\nu} + \delta T^{\mu}_{\nu} \\ &= \bar{T}^{\mu}_{\nu} + \begin{pmatrix} -\delta\rho & -(\bar{\rho} + \bar{p})(B_i - v_i) \\ (\bar{\rho} + \bar{p})(B_i - v_i) & \delta p\delta^{i}_{j} + \Pi^{i}_{j} \end{pmatrix} \end{aligned} \tag{3.32}$$

where we have used the conditions of the anisotropic stress tensor described in Equations 3.21 and $\bar{T}^{\mu}_{\nu}$ is the energy tensor of a perfect fluid defined in Equation 3.30.

For these types of decompositions into background and perturbation components to hold, we must be able to map a point on the background spacetime onto the perturbed spacetime of a given coordinate system. General relativity allows the freedom of choice of coordinate systems such that the physics remains invariant under coordinate (gauge) transformations and the consequences of attempting to map different spacetimes onto one another will be discussed in the following section.

3.2 Gauge Transformations

The theory of general relativity is covariant. This means that the physics is not affected by coordinate transformations. However, by using perturbation theory to describe quantities in terms of background and perturbation, the general covariance is broken.

For two sets of different coordinate systems in the perturbed spacetime $\hat{x}^{\alpha}$ and $\tilde{x}^{\alpha}$, we can relate these systems via a coordinate transformation given by

$$\tilde{x}^{\alpha} = \hat{x}^{\alpha} + \xi^{\alpha} \tag{3.33}$$

where ξ^α is a small (of linear order perturbations) gauge generator which we can think of as living in the background spacetime $\bar{x}^\alpha$ (Kurki-Suonio 2022).

Any given point on these perturbed spacetime coordinates are associated with a point on the background spacetime. Therefore, we can write

$$\hat{x}^\alpha(\hat{P}) = \tilde{x}^\alpha(\tilde{P}) = \bar{x}^\alpha(\bar{P}) \tag{3.34}$$

where the point P refers to an arbitrary point on its respective spacetime coordinates where we have mapped a point on the background spacetime ($\bar{P}$) onto a point on each of the coordinate systems in the perturbed spacetime.

We can then attempt to associate the points $\hat{P}$ and $\tilde{P}$ to alternative coordinates $\tilde{x}^\alpha$ and $\hat{x}^\alpha$ by using Equation 3.33 such that

$$\begin{aligned} \tilde{x}^\alpha(\hat{P}) &= \hat{x}^\alpha(\hat{P}) + \xi^\alpha \\ \hat{x}^\alpha(\tilde{P}) &= \tilde{x}^\alpha(\tilde{P}) - \xi^\alpha \end{aligned} \tag{3.35}$$

where $\tilde{x}^\alpha(\hat{P})$ is the point associated with $\hat{P}$ on coordinates $\tilde{x}^\alpha$ and $\hat{x}^\alpha(\tilde{P})$ similarly defined as such.

Differentiating the equations in 3.35 gives the gauge transformation matrices

$$\begin{aligned} \frac{\partial \tilde{x}^\alpha}{\partial \hat{x}^\beta} &= \delta^\alpha_\beta + \xi^\alpha{}_{,\beta} \\ \frac{\partial \hat{x}^\alpha}{\partial \tilde{x}^\beta} &= \delta^\alpha_\beta - \xi^\alpha{}_{,\beta} \end{aligned} \tag{3.36}$$

which does indeed satisfy the relation

$$\frac{\partial \tilde{x}^\alpha}{\partial \hat{x}^\beta}\frac{\partial \hat{x}^\beta}{\partial \tilde{x}^\gamma} = \delta^\alpha_\gamma \tag{3.37}$$

required for coordinate transformations to linear order in ξ^α.

We can also substitute Equation 3.34 into 3.35 to relate the position of the different points (associated with the same background point $\bar{P}$) on the same coordinate system

$$\begin{aligned} \tilde{x}^\alpha(\tilde{P}) &= \tilde{x}^\alpha(\hat{P}) - \xi^\alpha \\ \hat{x}^\alpha(\tilde{P}) &= \hat{x}^\alpha(\hat{P}) - \xi^\alpha \end{aligned} \tag{3.38}$$

From this, we can see that the mapping of two points associated with the same background point is the same in both coordinate systems. This implies that we do not have a unique mapping of a background quantity to the perturbed spacetime as in different gauges, the same point is associated with different points in the

background. As the perturbation of a quantity is defined as the difference between the perturbed and the background quantities, by definition, the perturbation is gauge-dependent.

For a 4-scalar $s = \bar{s} + \delta s$ in the perturbed spacetime, the perturbation δs exists in the background spacetime $\bar{x}^\alpha$ but is a gauge-dependent quantity. We can define the perturbation in the gauge associated with transformations from the background to $\hat{x}^\alpha$ coordinates as

$$\widehat{\delta s}(\bar{x}^\alpha) = s(\hat{P}) - \bar{s}(\bar{P}) \tag{3.39}$$

where $\widehat{\delta s}$ is the scalar perturbation in the background due to gauge and $s(\hat{P})$ is the scalar quantity in the $\hat{x}^\alpha$ coordinates at point $\hat{P}$. In this coordinate system, the scalar at $\tilde{P}$ is related to the scalar at $\hat{P}$ by

$$s(\tilde{P}) = s(\hat{P}) + \frac{\partial s(\hat{P})}{\partial \hat{x}^\alpha} \delta \hat{x}^\alpha \tag{3.40}$$

where $\delta \hat{x}^\alpha = \hat{x}^\alpha(\tilde{P}) - \hat{x}^\alpha(\hat{P})$ is the difference between the position of the points (Kurki-Suonio 2022). From Equation 3.38, we can see that $\delta \hat{x}^\alpha = -\xi^\alpha$.

The background coordinates can be expressed as $\bar{x}^\alpha = \hat{x}^\alpha + \xi^\alpha$ and therefore the transformation matrix can be written as

$$\frac{\partial \bar{x}^\alpha}{\partial \hat{x}^\beta} = \delta^\alpha_\beta + \xi^\alpha{}_{,\beta} \tag{3.41}$$

Looking at the derivative term in Equation 3.40, we can use Equation 3.39 and the transformation matrix above to write

$$\frac{\partial s(\hat{P})}{\partial \hat{x}^\alpha} = \frac{\partial}{\partial \hat{x}^\alpha} \left(\bar{s}(\bar{P}) + \widehat{\delta s}(\bar{x}^\alpha) \right) = \frac{\partial}{\partial \bar{x}^\beta} \left(\delta^\beta_\alpha + \xi^\beta{}_{,\alpha} \right) \left(\bar{s}(\bar{P}) + \widehat{\delta s}(\bar{x}^\alpha) \right) \tag{3.42}$$

Fortunately, as we multiply this by ξ^α (which is of first order in perturbation) in Equation 3.40 and we are considering linear order perturbations, we can ignore all perturbation terms. Furthermore, as the background is only a function of conformal time, we can simplify this further to give

$$\frac{\partial s(\hat{P})}{\partial \hat{x}^\alpha} \approx \frac{\partial \bar{s}(\bar{P})}{\partial \bar{x}^\alpha} = \bar{s}' \tag{3.43}$$

We can substitute these results into Equation 3.40 to find

$$s(\tilde{P}) = s(\hat{P}) - \bar{s}' \xi^0 \tag{3.44}$$

Similarly to Equation 3.39, we can define an equation for the scalar perturbations in the $\tilde{x}^\alpha$ gauge

$$\widetilde{\delta s}(\bar{x}^\alpha) = s(\tilde{P}) - \bar{s}(\bar{P}) \tag{3.45}$$

We can substitute Equation 3.44 to find

$$\widetilde{\delta s}(\bar{x}^\alpha) = s(\hat{P}) - \bar{s}'\xi^0 - \bar{s}(\bar{P}) \tag{3.46}$$

we can then use Equation 3.39 again to relate the scalar perturbations in different gauges

$$\widetilde{\delta s}(\bar{x}^\alpha) = \widehat{\delta s}(\bar{x}^\alpha) - \bar{s}'\xi^0 \tag{3.47}$$

Now that we understand how a 4-scalar transforms under different gauges, we can apply the same method for a four-vector in the perturbed spacetime defined as

$$\begin{aligned} \hat{v}^\alpha(\hat{P}) &= \bar{v}^\alpha(\bar{P}) + \widehat{\delta v}^{\,\alpha}(\bar{x}^\beta) \\ \tilde{v}^\alpha(\tilde{P}) &= \bar{v}^\alpha(\bar{P}) + \widetilde{\delta v}^{\,\alpha}(\bar{x}^\beta) \end{aligned} \tag{3.48}$$

where the δv^α are the perturbations of the vector quantity that exists in the background but is dependent on the gauge choice.

Similar to Equation 3.40, we can formulate an equation to relate $\hat{v}^\alpha(\tilde{P})$ to $\hat{v}^\alpha(\hat{P})$ such that

$$\hat{v}^\alpha(\tilde{P}) = \hat{v}^\alpha(\hat{P}) - \xi^\beta \frac{\partial \hat{v}^\alpha(\hat{P})}{\partial \hat{x}^\beta} = \hat{v}^\alpha(\hat{P}) - \bar{v}^\alpha{}_{,\beta}\,(\bar{P})\xi^\beta \tag{3.49}$$

to linear order in perturbations.

To write an equation linking vector perturbations of different gauges, we can transform between coordinates using the transformation matrix in Equation 3.36 so that

$$\tilde{v}^\alpha(\tilde{P}) = \frac{\partial \tilde{x}^\alpha}{\partial \hat{x}^\gamma}\hat{v}^\gamma(\tilde{P}) = \left(\delta^\alpha_\gamma + \xi^\alpha{}_{,\gamma}\right)\left(\hat{v}^\gamma(\hat{P}) - \bar{v}^\gamma{}_{,\beta}\,(\bar{P})\xi^\beta\right) \tag{3.50}$$

where we have substituted Equation 3.49 for $\hat{v}^\gamma(\tilde{P})$. Substituting the linear order terms in this result into Equation 3.48 gives

$$\widetilde{\delta v}^{\,\alpha} = \widehat{\delta v}^{\,\alpha} + \xi^\alpha{}_{,\beta}\,\bar{v}^\beta - \bar{v}^\alpha{}_{,\beta}\,\xi^\beta \tag{3.51}$$

If the background $\bar{v}^\alpha(\eta)$ is a function of conformal time only we can separate the result above into

$$\begin{aligned} \widetilde{\delta v}^{\,0} &= \widehat{\delta v}^{\,0} + \xi^0{}_{,0}\,\bar{v}^0 - \bar{v}^0{}_{,0}\,\xi^0 \\ \widetilde{\delta v}^{\,i} &= \widehat{\delta v}^{\,i} + \xi^i{}_{,0}\,\bar{v}^0 \end{aligned} \tag{3.52}$$

Finally, for a tensor $t_{\alpha\beta}$ we have

$$\begin{aligned}\hat{t}_{\alpha\beta}(\hat{P}) &= \bar{t}_{\alpha\beta}(\bar{P}) + \hat{\delta}t_{\alpha\beta}(\bar{x}^\gamma) \\ \tilde{t}_{\alpha\beta}(\tilde{P}) &= \bar{t}_{\alpha\beta}(\bar{P}) + \tilde{\delta}t_{\alpha\beta}(\bar{x}^\gamma)\end{aligned} \tag{3.53}$$

Following the same approach as the scalar and vector perturbations, we can associate the tensor perturbations of different gauges by finding $\tilde{t}_{\alpha\beta}(\tilde{P})$ as a function of $\hat{t}_{\alpha\beta}(\hat{P})$. Using the transformation matrices in Equation 3.36, we have

$$\begin{aligned}\tilde{t}_{\alpha\beta}(\tilde{P}) &= \left(\hat{t}_{\mu\nu}(\hat{P}) - \xi^\gamma \frac{\partial \bar{t}_{\mu\nu}(\bar{P})}{\partial \bar{x}^\gamma}\right)\left(\delta^\mu_\alpha - \xi^\mu{}_{,\alpha}\right)\left(\delta^\nu_\beta - \xi^\nu{}_{,\beta}\right) \\ &= \hat{t}_{\alpha\beta}(\hat{P}) - \xi^\mu{}_{,\alpha}\,\bar{t}_{\mu\beta}(\bar{P}) - \bar{t}_{\alpha\nu}(\bar{P})\xi^\nu{}_{,\beta} - \bar{t}_{\alpha\beta,0}\,\xi^0\end{aligned} \tag{3.54}$$

where in the final step we have linearised the equation in perturbations and used the fact that the background tensor $\bar{t}_{\alpha\beta}$ will only have non-zero derivatives in time only.

3.3 Decomposition

In Equation 3.12, we represented the perturbation to the metric tensor in terms of the scalar lapse function (A) in δg_{00}, a 3D shift vector (B_i) in δg_{0i} and the spatial perturbation (C_{ij}) in δg_{ij}. We understand that under different gauges, these terms will transform according to the rules determined in the previous section.

However, before this, we can use the Helmholtz decomposition theorem to rewrite the 3-vector and the 3D rank 2 tensor into scalar, vector and tensor components. Starting with the 3-vector, the theorem states that we can resolve a well behaved vector field into a sum of a transverse (divergence-free) and the divergence of a scalar field (curl-free). Therefore, we can write

$$B_i = B_i^{\parallel} + B_i^{\perp} = -B_{,i} + S_i \tag{3.55}$$

where $B_i^{\parallel} = -B_{,i}$ is the gradient of a scalar field B and $B_i^{\perp} = S_i$ is the divergence-free ($S^k{}_{,k} = 0$) vector field. The negative sign arises from the consideration of B as a potential of the vector field $B_i^{\parallel}$. While the symbols are taken from Malik (2023), due to this sign choice, the terms differ by -1 to Malik (2023) which is the reason for the inclusion of the additional negative sign in the vector component of the metric perturbation (which makes the scalar of B_i positive).

In similar fashion, we can attempt to decompose the tensor C_{ij}. We can begin by

splitting this into trace and traceless tensors as shown below

$$C_{ij} = \frac{1}{3}\delta_{ij}\delta^{kl}C_{kl} + E_{ij} \tag{3.56}$$

where $\delta^{kl}C_{kl} = C^k_k$ is the trace of tensor C_{ij} and E_{ij} is the traceless tensor. For the traceless tensor E_{ij}, we can decompose it into scalar, vector and tensor components such that

$$E_{ij} = E^{\parallel}_{ij} + E^{\perp}_{ij} + E^{T}_{ij} \tag{3.57}$$

where

$$E^{\parallel}_{ij} = E_{,ij} - \frac{1}{3}\delta_{ij}\delta^{kl}E_{,kl} \tag{3.58}$$

where E is a scalar field,

$$E^{\perp}_{ij} = -\frac{1}{2}\left(E_{i,j} + E_{j,i}\right) \tag{3.59}$$

where E_i is a divergence-free vector field and E^T_{ij} is a symmetric, divergence-free and traceless tensor (Kurki-Suonio 2022). Using notation used in Malik (2023), we can write Equation 3.57 as

$$C_{ij} = -\psi\delta_{ij} + E_{,ij} + \frac{1}{2}\left(F_{i,j} + F_{j,i}\right) + \frac{1}{2}h_{ij} \tag{3.60}$$

where $\psi = 1/3(E^{,k}_{,k} - C^k_k)$ is the curvature perturbation and we have defined $F_i = -E_i$ and $h_{ij} = 2E^T_{ij}$.

Substituting these results into the metric perturbation in Equation 3.12, we have

$$\delta g_{\mu\nu} = a^2 \begin{pmatrix} -2\phi & B_{,i} - S_i \\ B_{,i} - S_i & 2(-\psi\delta_{ij} + E_{,ij}) + F_{i,j} + F_{j,i} + h_{ij} \end{pmatrix} \tag{3.61}$$

where we have used $\phi = A$ from Malik (2023).

This is useful as for linear order perturbations, the scalar, vector and tensor components are decoupled and so can be treated independently of one another.

We can also decompose the 3-velocity vector perturbation defined in Equation 3.26 so that we can write

$$v_i = v^{\parallel}_i + v^{\perp}_i = -v_{,i} + v^{\perp}_i \tag{3.62}$$

where $\delta^{ik}v^{\perp}_{k,i} = 0$ and v is the 3-velocity field. Therefore, we can write our perturbed

4-velocity vectors as

$$\begin{aligned} u^\mu &= \frac{1}{a}(1-\phi, v_i^\perp - v_{,i}) \\ u_\mu &= -a(1+\phi, v_{,i} - B_{,i} + S_i - v_i^\perp) \end{aligned} \tag{3.63}$$

By definition, the anisotropic stress tensor is traceless. Therefore, we can perform the same decomposition as the tensor E_{ij} so that

$$\begin{aligned} \Pi_{ij} &= \Pi_{ij}^{\parallel} + \Pi_{ij}^{\perp} + \Pi_{ij}^{T} \\ &= \Pi_{,ij} - \frac{1}{3}\delta_{ij}\delta^{kl}\Pi_{,kl} - \frac{1}{2}(\Pi_{i,j} + \Pi_{j,i}) + \Pi_{ij}^{T} \end{aligned} \tag{3.64}$$

where we have broken down the covariant tensor into scalar (Π), vector (Π_i) and tensor (Π_{ij}^T) components. By raising an index on the covariant stress-energy tensor, we can see that $\Pi_j^i = a^{-2}\delta^{ik}\Pi_{kj}$ as it is a pure perturbation term.

The covariant form of the energy tensor is given by

$$\begin{aligned} T_{\mu\nu} &= g_{\mu\alpha}T_\nu^\alpha = (\rho + p)u_\mu u_\nu + p g_{\mu\nu} + \Pi_{\mu\nu} \\ &= \bar{T}_{\mu\nu} + a^2 \begin{pmatrix} \delta\rho + 2\phi\bar{\rho} & (\bar{\rho}+\bar{p})(B_i - v_i) - B_i\bar{p} \\ (\bar{\rho}+\bar{p})(B_i - v_i) - B_i\bar{p} & \delta p\delta_{ij} + \Pi_{ij} + 2C_{ij}\bar{p} \end{pmatrix} \end{aligned} \tag{3.65}$$

where T_ν^α is the stress energy tensor given in Equation 3.32 and $\bar{T}_{\mu\nu}$ is the background stress energy tensor in Equation 3.29. We can now decompose the perturbation of the stress energy tensor into scalar, vector and tensor components so that

$$\begin{aligned} \delta T_{00} &= a^2(\delta\rho + 2\phi\bar{\rho}) \\ \delta T_{0i} &= a^2[(\bar{\rho}+\bar{p})(v-B)_{,i} + B_{,i}\,\bar{p}] + a^2[(\bar{\rho}+\bar{p})(S_i - v_i^\perp) - S_i\bar{p}] \\ \delta T_{ij} &= a^2\left[\left(\delta p - 2\bar{p}\psi - \frac{1}{3}\delta^{kl}\Pi_{,kl}\right)\delta_{ij} + (2\bar{p}E + \Pi)_{,ij}\right] \\ &\quad + a^2\left[\left(\bar{p}F_i - \frac{1}{2}\Pi_i\right)_{,j} + \left(\bar{p}F_j - \frac{1}{2}\Pi_j\right)_{,i}\right] \\ &\quad + a^2[h_{ij}\bar{p} + \Pi_{ij}^T] \end{aligned} \tag{3.66}$$

We can also perform the same procedure for our arbitrary gauge generator $\xi^\alpha = \xi^0 + \xi^i$. We can decompose the 3-vector component into

$$\xi^i = -\xi_{,j}\,\delta^{ij} + \xi_\perp^i \tag{3.67}$$

which will prove to be useful in the following section.

3.4 Gauge Transformation of Perturbations

The linear perturbation in the metric tensor ($\delta g_{\mu\nu}$) will evolve according to Equation 3.54 under gauge transformations. Using our definition of the background metric tensor ($\bar{g}_{\mu\nu} = a^2\eta_{\mu\nu}$) given in Equation 3.4, the transformed metric is

$$\widetilde{\delta g}_{\mu\nu} = \delta g_{\mu\nu} - a^2\left(\xi^{\alpha}{}_{,\mu}\,\eta_{\alpha\nu} + \eta_{\mu\beta}\xi^{\beta}{}_{,\nu} + 2\frac{a'}{a}\eta_{\mu\nu}\xi^0\right) \tag{3.68}$$

where we have chosen to remove the $\hat{}$ on the original metric tensor perturbation and $\eta_{\mu\nu}$ is the Minkowski metric.

But we have also defined the metric tensor perturbations in terms of scalar, vector and tensor quantities in Equation 3.61. For each of these terms, we can use Equation 3.79 to obtain their gauge transformation laws.

The transformation of δg_{00} under a gauge transformation can be written as

$$\widetilde{\delta g}_{00} = -2a^2\tilde{\phi} = -2a^2\phi - a^2\left(\xi^{\alpha}{}_{,0}\,\eta_{\alpha 0} + \eta_{0\beta}\xi^{\beta}{}_{,0} + 2\mathcal{H}\eta_{00}\xi^0\right) \tag{3.69}$$

and so we can simplify to obtain

$$\tilde{\phi} = \phi - \xi^{0\prime} - \mathcal{H}\xi^0 \tag{3.70}$$

using the partial derivative notation defined in Equation 3.7. Compared to the result in Malik (2023), we note the opposing sign convention in the transformations due to the difference in the signs of the definitions of the coordinate transformation.

Similarly, the $0i$ components can be substituted to find

$$\begin{aligned}\tilde{B}_{,i} - \tilde{S}_i &= B_{,i} - S_i - (\xi_{i,0} - \xi_{0,i}) \\ &= B_{,i} - S_i - \left(-\xi_{,i0} + \xi_i^{\perp}{}_{,0} - \xi_{0,i}\right)\end{aligned} \tag{3.71}$$

where we have used the decomposition of the spatial components of the gauge generator ξ^i in Equation 3.67 in the second line. By collecting and comparing the divergence terms, we get the results

$$\tilde{B} = B + \xi' + \xi_0 \tag{3.72}$$

and

$$\tilde{S}_i = S_i + \xi_{\perp}^{i\,\prime} \tag{3.73}$$

for the vector components, again using the same time derivative notation.

Finally, for the spatial components, we have

$$\begin{aligned}\widetilde{\delta g}_{ij} &= \delta g_{ij} - a^2\left[\xi_{j,i} + \xi_{i,j} + 2\mathcal{H}\delta_{ij}\xi^0\right] \\ &= a^2\Big\{2\left(-\psi\delta_{ij} + E_{,ij}\right) + F_{i,j} + F_{j,i} + h_{ij} \\ &\quad - \left[\left(-\xi_{,j} + \xi_j^{\perp}\right)_{,i} + \left(-\xi_{,i} + \xi_i^{\perp}\right)_{,j} + 2\mathcal{H}\xi^0\delta_{ij}\right]\Big\}\end{aligned} \tag{3.74}$$

where we have again used the spatial decomposition of ξ^i in the second equality. We can now separate and collect the variables into scalar, vector and tensor terms to find the relevant transformation rules to be

$$\tilde{\psi} = \psi + \mathcal{H}\xi^0 \tag{3.75}$$

and

$$\tilde{E} = E + \xi \tag{3.76}$$

for the scalars ψ and E,

$$\tilde{F}_i = F_i - \xi_i^{\perp} \tag{3.77}$$

as $F_{i,j} = F_{j,i}$ by the nature of the construction of the $E_{ij}^{\perp}$ matrix from Equation 3.57 and the tensor h_{ij} is invariant under gauge transformations.

Therefore, for a perturbed metric tensor given by

$$\begin{aligned}g_{\mu\nu} &= a^2\eta_{\mu\nu} + \delta g_{\mu\nu} \\ &= a^2\begin{pmatrix} -(1+2\phi) & B_{,i} - S_i \\ B_{,i} - S_i & (1-2\psi)\delta_{ij} + 2E_{,ij} + F_{i,j} + F_{j,i} + h_{ij}\end{pmatrix}\end{aligned} \tag{3.78}$$

we can write its transformation under an arbitrary gauge $\xi^{\alpha} = \xi^0 - \xi,^i + \xi_{\perp}^i$ as

$$\begin{aligned}\widetilde{g}_{\mu\nu} = g_{\mu\nu} + a^2\Bigg[&\begin{pmatrix} 2(\xi^{0\prime} + \mathcal{H}\xi^0) & \xi',_i + \xi^0,_i \\ \xi',_i + \xi^0,_i & 2(-\mathcal{H}\xi^0\delta_{ij} + \xi,_{ij})\end{pmatrix} \\ &+ \begin{pmatrix} 0 & -\xi_{\perp}^{i\,\prime} \\ -\xi_{\perp}^{i\,\prime} & -\left(\xi_j^{\perp},_i + \xi_i^{\perp},_j\right)\end{pmatrix}\Bigg]\end{aligned} \tag{3.79}$$

where we have split the components added due to the gauge transformations into scalar, vector and tensor quantities (noting that the tensor is invariant under gauge transformations).

The matter variables can also be transformed under a gauge. The scalar quantities of $\rho = \bar{\rho} + \delta\rho$ and $p = \bar{p} + \delta p$ transform using the scalar transformation rule given

in Equation 3.47. Therefore, we can write their perturbations as

$$\widetilde{\delta\rho} = \delta\rho - \bar{\rho}'\xi^0 \tag{3.80}$$

and

$$\widetilde{\delta p} = \delta p - \bar{p}'\xi^0 \tag{3.81}$$

respectively.

We can use the 4-vector transformation rule in Equation 3.52 to find the transformation of the 3-velocity perturbation. We can decompose this into the scalar and vector components defined in Equation 3.62 which transform as

$$\begin{aligned} \tilde{v} &= v + \xi' \\ \tilde{v}_i^{\perp} &= v_i^{\perp} + \xi_i^{\perp\prime} \end{aligned} \tag{3.82}$$

where we have also decomposed the gauge generator into its scalar and vector components.

Finally, the transformation of the anisotropic stress tensor can be found by considering the ij spatial components of the tensor transformation rule in Equation 3.54. Doing this, we can see that in fact Π_{ij} is a gauge invariant quantity as it has no background quantity and so

$$\tilde{\Pi}_{ij} = \Pi_{ij} \tag{3.83}$$

We can also define the density contrast $\delta = \delta\rho/\bar{\rho}$. This dimensionless parameter will transform under a gauge transform as

$$\tilde{\delta} = \delta - \frac{\bar{\rho}'}{\bar{\rho}}\xi^0 = \delta + 3\mathcal{H}(1+w)\xi^0 \tag{3.84}$$

where we have used the transformation rule of $\delta\rho$ in Equation 3.80 and the energy continuity equation in Equation 1.6.

The separation of quantities into scalar, vector and tensor components and finding their individual gauge transformation rules is useful at linear order perturbations as each component evolves independently to one another. Therefore, we can consider each variable separately (particularly the scalar perturbations).

3.5 Fourier Modes of Perturbations

Another convenient consequence of linear perturbation theory is that we can expand the perturbations into Fourier modes where at linear order, each mode evolves independently of one another (Kurki-Suonio 2022). We can expand these perturbations into modes of a comoving wave vector $\mathbf{k}$ where the comoving wavenumber (k) and wavelength (λ) are related to their physical quantities by

$$k_{phys} = \frac{2\pi}{\lambda_{phys}} = \frac{2\pi}{a\lambda} = \frac{k}{a} \tag{3.85}$$

from Kurki-Suonio (2022).

For a perturbation $f = f(x^\mu)$ in coordinate space $x^\mu = (\eta, x^i)$, we can use the convention used in Kurki-Suonio (2022) to write

$$f(\eta, \mathbf{x}) = \sum_{\mathbf{k}} \frac{f_{\mathbf{k}}(\eta)}{k^n} e^{i\mathbf{k}\cdot\mathbf{x}} \tag{3.86}$$

where $i = \sqrt{-1}$, $f_{\mathbf{k}}(\eta)$ is the Fourier mode of f for a given wave vector $\mathbf{k}$ and n is an integer to denote the convention used in Kurki-Suonio (2022) which divides each mode by powers of k to ensure that all the metric perturbations have the same dimensions in Fourier space. This is shown in Table 3.2 where we can see for example that ξ gains a factor of $1/k$ due to the spatial derivative in Equation 3.67.

Table 3.2: Examples of the convention used to denote Fourier modes used Kurki-Suonio (2022). A factor of $1/k$ enters for each spatial derivative in the definition of the quantity.

Quantities	ϕ	B	ξ	Π	E
n	0	1	1	2	2

In Fourier space, we can write

$$\partial_j \to ik_j \tag{3.87}$$

where again $i = \sqrt{-1}$ and j denote the spatial indices. So our variables in Fourier space are solely a function of conformal time for a given wave vector.

We can now rewrite the metric perturbations and their gauge transform in Fourier space. The transformation rules of each perturbation in Fourier space is shown on Table 3.3. This allows us to now rewrite the gauge transform of the perturbations

Table 3.3: The metric perturbation variables and their transformation rules in coordinate and Fourier space.

Perturbations	Transformation in coordinate space	Transformation of Fourier mode
ϕ	$-(\xi^{0\prime} + \mathcal{H}\xi^0)$	$-(\xi^{0\prime} + \mathcal{H}\xi^0)$
B	$\xi' + \xi_0$	$\xi' + k\xi_0$
ψ	$\mathcal{H}\xi^0$	$\mathcal{H}\xi^0$
E	ξ	$k\xi$
S_i	$\xi_\perp^{i\,\prime}$	$\xi_\perp^{i\,\prime}$
F_i	$-\xi_i^\perp$	$-k\xi_i^\perp$
h_{ij}	0	0

of the metric tensor as

$$\widetilde{\delta g}_{\mu\nu} = a^2 \Bigg[\begin{pmatrix} -2\phi & i\frac{k_j}{k}B - S_j \\ i\frac{k_j}{k}B - S_j & 2\left(-\psi\delta_{jl} - \frac{k_j k_l}{k^2}E\right) + i\frac{k_l}{k}F_j + i\frac{k_j}{k}F_l + h_{jl} \end{pmatrix} + \begin{pmatrix} 2(\xi^{0\prime} + \mathcal{H}\xi^0) & i\frac{k_j}{k}\left(\xi' + k\xi^0\right) \\ i\frac{k_j}{k}\left(\xi' + k\xi^0\right) & 2\left(-\mathcal{H}\xi^0\delta_{jl} - \frac{k_j k_l}{k}\xi\right) \end{pmatrix} + \begin{pmatrix} 0 & -\xi_\perp^{j\,\prime} \\ -\xi_\perp^{j\,\prime} & -i\left(k_l\xi_j^\perp + k_j\xi_i^\perp\right) \end{pmatrix} \Bigg] \tag{3.88}$$

where the first matrix is the gauge perturbation $\delta g_{\mu\nu}$ in Fourier space, the second is the additional scalar terms due to gauge transformations and the final matrix contains the vector terms.

As mentioned in Malik (2023), the scalar perturbations couple to perturbations in density and pressure and evolve such perturbations. Therefore, in this dissertation, we will focus on the effects of the scalar perturbations ϕ, B, ψ and E. Under a general gauge transform ξ^α, the transformation of these scalars can be described in terms of scalars ξ^0 and ξ.

3.6 Newtonian Gauge

The gauge generator is an arbitrary 4-vector. Therefore, we can introduce two constraints to the perturbations by fixing the gauge variables to specific quantities. Choosing these gauges allows us to eliminate two perturbations, allowing us to solve the perturbed Einstein equations.

In Newtonian gauge, we eliminate scalar variables E and B by choosing

$$\begin{aligned} \xi^0 &= -B + E' \\ \xi &= -E \end{aligned} \tag{3.89}$$

in coordinate space. We can also create two gauge invariant variables using the scalar variables ϕ, B, E and ψ known as the Bardeen potentials:

$$\Phi = \phi + \mathcal{H}(B - E') + (B - E')' \tag{3.90}$$

and

$$\Psi = \psi - \mathcal{H}(B - E') \tag{3.91}$$

in coordinate space Belušević (2008). In Newtonian gauge, these Bardeen potentials become ϕ and ψ. Therefore, we can write our scalar perturbed metric and its inverse as

$$\begin{aligned} g_{\mu\nu} &= a^2 \begin{pmatrix} -(1+2\Phi) & 0 \\ 0 & (1-2\Psi)\delta_{ij} \end{pmatrix} \\ g^{\mu\nu} &= a^{-2} \begin{pmatrix} -1+2\Phi & 0 \\ 0 & (1+2\Psi)\delta_{ij} \end{pmatrix} \end{aligned} \tag{3.92}$$

respectively in Newtonian gauge.

We can use these co and contravariant metrics to find the Christoffel symbols in the Newtonian gauge using Equation 3.18. The obtained Christoffel symbols can be split into background and linear order perturbation components as shown on Table 3.4.

Table 3.4: Background and linear perturbations of the Christoffel symbol in Newtonian gauge for perturbations to the metric tensor.

$\Gamma^\alpha_{\mu\nu}$	$\bar{\Gamma}^\alpha_{\mu\nu}$	$\delta\Gamma^\alpha_{\mu\nu}$
Γ^0_{00}	$\mathcal{H}$	Φ'
Γ^0_{0j}	0	$\Phi_{,j}$
Γ^0_{ij}	$\mathcal{H}\delta_{ij}$	$-[2\mathcal{H}(\Phi+\Psi)+\Psi']\delta_{ij}$
Γ^k_{00}	0	$\Phi_{,k}$
Γ^k_{0j}	$\mathcal{H}\delta^i_j$	$-\Psi'\delta^i_j$
Γ^k_{ij}	0	$-(\Psi_{,j}\,\delta^k_i + \Psi_{,i}\,\delta^k_j) + \Psi_{,k}\,\delta_{ij}$

We can then use the results in Table 3.4 to find the perturbed Ricci tensor using Equation 3.17 which can also be split into the background and linear perturbation

components

$$
\begin{aligned}
R_{\mu\nu} &= \bar{R}_{\mu\nu} + \delta R_{\mu\nu} \\
&\begin{pmatrix} -3\mathcal{H}' & 0 \\ 0 & (\mathcal{H}' + 2\mathcal{H}^2)\delta_{ij} \end{pmatrix} \\
&+ \begin{pmatrix} 3\Psi'' + \Phi_{,kl}\,\delta^{kl} + 3\mathcal{H}(\Phi + \Psi)' & 2(\Psi + \mathcal{H}\Phi)_{,i} \\ 2(\Psi + \mathcal{H}\Phi)_{,i} & [-\Psi'' + \Psi_{,kl}\,\delta^{kl} - \mathcal{H}(\Phi + 5\Psi)' \\ & -(2\mathcal{H}' + 4\mathcal{H}^2)(\Phi + \Psi)]\delta_{ij} + (\Psi - \Phi)_{,ij} \end{pmatrix}
\end{aligned}
\tag{3.93}
$$

To find the Einstein tensor, we need the trace of the Ricci tensor which is also known as the Ricci scalar

$$
\begin{aligned}
R^{\lambda}_{\lambda} &= R^0_0 + R^i_i \\
&= g^{0\mu} R_{\mu 0} + g^{i\mu} R_{\mu i} \\
&= \bar{g}^{00}\bar{R}_{00} + \bar{g}^{00}\delta R_{00} + \delta g^{00}\bar{R}_{00} + \bar{g}^{ij}\bar{R}_{ji} + \bar{g}^{ij}\delta R_{ji} + \delta g^{ij}\bar{R}_{ji} \\
&= a^{-2}[6\mathcal{H}' + 6\mathcal{H}^2 - 6\Psi'' + 2(2\Psi - \Phi)_{,kl}\,\delta^{kl} \\
&- 6\mathcal{H}(\Phi + 3\Psi)' - 12(\mathcal{H}' + \mathcal{H}^2)\Phi]
\end{aligned}
\tag{3.94}
$$

where we have raised the index using the inverse metric in Equation 3.92 and multiplied out to first order in perturbations. Using this, we can now derive the left hand side of Equation 3.15 by using the definition of the Einstein tensor given in Equation 3.16

$$
\begin{aligned}
G_{\mu\nu} &= \bar{G}_{\mu\nu} + \delta G_{\mu\nu} \\
&= \begin{pmatrix} 3\mathcal{H}^2 & 0 \\ 0 & -(2\mathcal{H}' + \mathcal{H}^2)\delta_{ij} \end{pmatrix} \\
&+ \begin{pmatrix} 2(\Psi_{,kl}\,\delta^{kl} - 3\mathcal{H}\Psi') & 2(\Psi + \mathcal{H}\Phi)_{,i} \\ 2(\Psi + \mathcal{H}\Phi)_{,i} & [2\Psi'' + (\Phi - \Psi)_{,kl}\,\delta^{kl} + 2\mathcal{H}(\Phi + 2\Psi)' \\ & +2(2\mathcal{H}' + \mathcal{H}^2)\Phi - 2\Psi(4\mathcal{H}' + 5\mathcal{H}^2)]\delta_{ij} + (\Psi - \Phi)_{,ij} \end{pmatrix}
\end{aligned}
\tag{3.95}
$$

The scalar perturbations of the energy tensor can be written as

$$
\delta T^{\mu}_{\nu} = \begin{pmatrix} -\delta\rho & (\bar{\rho} + \bar{p})(B - v)_{,i} \\ (\bar{\rho} + \bar{p})(v - B)_{,i} & \delta p\,\delta^i_j + \Pi^i_j \end{pmatrix} \tag{3.96}
$$

and so we have the first order perturbations of the Einstein equations as

$$\begin{aligned} a^{-2}[\Psi_{,kl}\,\delta^{kl} - 3\mathcal{H}(\Psi' + \mathcal{H}\Phi)] &= 4\pi G\delta\rho \\ a^{-2}(\Psi' + \mathcal{H}\Phi)_{,i} &= 4\pi G(\bar{\rho} + \bar{p})v_{,i} \\ a^{-2}\{2[\Psi'' + (\Phi - \Psi)_{,kl}\,\delta^{kl} + \mathcal{H}(\Phi + 2\Psi)' + \\ \Phi(2\mathcal{H}' + \mathcal{H}^2)]\delta^i_j + (\Psi - \Phi)_{,ij}\} &= 8\pi G a^2\bar{p}(\Pi_{,ij} - \frac{1}{3}\delta^i_j\Pi_{,kl}\,\delta^{kl}) \end{aligned} \tag{3.97}$$

(Kurki-Suonio 2022) in Newtonian gauge such that $B = 0$.

With the perturbed Einstein equations, we can solve for the evolution of different perturbations by solving the background Friedmann equation (Equation 3.5) to obtain background quantities (such as $\mathcal{H}$) as a function of η. We can then substitute this into the Einstein equations to solve for the perturbations.

3.7 Sachs-Wolfe Effect

For photons travelling through spacetime, their motion follows the geodesic equation in Equation 3.22. We can define the affine parameter λ such that

$$P^\mu = \frac{\mathrm{d}x^\mu}{\mathrm{d}\lambda} \tag{3.98}$$

where P^μ is the photon 4-momentum (Kurki-Suonio 2022). This allows us to re-write the geodesic as

$$\frac{\mathrm{d}P^\mu}{\mathrm{d}\lambda} + \Gamma^\mu_{\alpha\beta}P^\alpha P^\beta = 0 \tag{3.99}$$

We can separate this into chronal ($\mu = 0$) and spatial ($\mu = k$) components

$$\begin{aligned} \frac{\mathrm{d}P^0}{\mathrm{d}\lambda} + \Gamma^0_{00}(P^0)^2 + 2\Gamma^0_{0l}P^0P^l + \Gamma^0_{ij}P^iP^j = 0 \\ \frac{\mathrm{d}P^k}{\mathrm{d}\lambda} + \Gamma^k_{00}(P^0)^2 + 2\Gamma^k_{0l}P^0P^l + \Gamma^k_{ij}P^iP^j = 0 \end{aligned} \tag{3.100}$$

As we are concerned with the energy of the photons from the formation of the CMB (P^0) we can consider the first equation.

To write the equation in terms of conformal time, we can use $P^0 = \mathrm{d}\eta/\mathrm{d}\lambda$ from Equation 3.98 to obtain

$$\frac{\mathrm{d}P^0}{\mathrm{d}\eta} + \Gamma^0_{00}P^0 + 2\Gamma^0_{0l}P^l + \Gamma^0_{ij}\frac{P^iP^j}{P^0} = 0 \tag{3.101}$$

We can now substitute the perturbed Christoffel symbols in the Newtonian gauge given in Table 3.4 to get

$$\frac{\mathrm{d}P^0}{\mathrm{d}\eta} + (\mathcal{H} + \Phi')P^0 + 2\Phi_{,l}\,P^l + [\mathcal{H} - 2\mathcal{H}(\Phi + \Psi) - \Psi']\delta_{ij}\frac{P^iP^j}{P^0} = 0 \tag{3.102}$$

For a photon propagating along the geodesic, we know that

$$P^2 = g_{\mu\nu}P^\mu P^\nu = g_{00}(P^0)^2 + g_{ij}P^iP^j = 0 \tag{3.103}$$

as it is a null geodesic (Belušević 2008). The second term in the equation above is the square of the 3-momentum ($\delta_{ij}p^ip^j$) and so we can express the 4-momenta components in terms of the 3-momenta

$$\begin{aligned} a^2(1 + 2\Phi)(P^0)^2 &= p^2 \\ a^2(1 - 2\Psi)\delta_{ij}P^iP^j &= \delta_{ij}p^ip^j \end{aligned} \tag{3.104}$$

where we have used the metric tensor in Newtonian gauge (Equation 3.92). Rearranging for the 4-momenta components to linear order in perturbation, we get

$$\begin{aligned} P^0 &= (1 + 2\Phi)^{-1/2}\frac{p}{a} = (1 - \Phi)\frac{p}{a} \\ P^i &= (1 - 2\Psi)^{-1/2}\frac{p^i}{a} = (1 + \Psi)\frac{p}{a}n^i \end{aligned} \tag{3.105}$$

where n^i is the directional unit vector of the 3-momenta ($p^i = pn^i$). Substituting the equation above into Equation 3.102 and rearranging for $\mathrm{d}P^0/\mathrm{d}\eta$ we have

$$\begin{aligned} \frac{\mathrm{d}P^0}{\mathrm{d}\eta} &= -(\mathcal{H} + \Phi')(1 - \Phi)\frac{p}{a} - 2\Phi_{,l}\,(1 + \Psi)\frac{p}{a}n^l - [\mathcal{H} - 2\mathcal{H}(\Phi + \Psi) - \Psi']\frac{(1 + \Psi)^2}{(1 - \Phi)}\frac{p}{a} \\ &= \frac{p}{a}\{-(\mathcal{H} - \mathcal{H}\Phi + \Phi') - 2\Phi_{,l}\,n^l - [\mathcal{H} - 2\mathcal{H}(\Phi + \Psi) - \Psi'](1 + 2\Psi)(1 + \Phi)\} \\ &= \frac{p}{a}\{\Psi' - \Phi' - 2\Phi_{,l}\,n^l - 2\mathcal{H}(1 - \Phi)\} \end{aligned} \tag{3.106}$$

to first order in perturbations.

We can also substitute for P^0 on the LHS which becomes

$$\begin{aligned} \frac{\mathrm{d}P^0}{\mathrm{d}\eta} &= \frac{\mathrm{d}}{\mathrm{d}\eta}\left[\frac{p}{a}(1 - \Phi)\right] \\ &= \frac{1}{a}\frac{\mathrm{d}p}{\mathrm{d}\eta}(1 - \Phi) - \frac{p}{a}\frac{\mathrm{d}\Phi}{\mathrm{d}\eta} - \frac{p}{a}\mathcal{H}(1 - \Phi) \end{aligned} \tag{3.107}$$

which we can substitute into Equation 3.106 and rearrange to get

$$\frac{1}{p}\frac{\mathrm{d}p}{\mathrm{d}\eta} = \frac{\mathrm{d}\Phi}{\mathrm{d}\eta} - \mathcal{H} + \Psi' - \Phi' - 2\Phi_{,l}\, n^l \tag{3.108}$$

For the first term on the RHS, we can write

$$\begin{aligned}\frac{\mathrm{d}\Phi}{\mathrm{d}\eta} &= \frac{\partial\Phi}{\partial\eta} + \frac{\partial\Phi}{x^i}\frac{\partial x^i}{\partial\eta} \\ &= \Phi' + \Phi_{,i}\,\frac{\partial x^i}{\partial\lambda}\frac{\partial\lambda}{\partial\eta} \\ &= \Phi' + \Phi_{,i}\,\frac{P^i}{P^0} = \Phi' + \Phi_{,i}\, n^i(1+\Psi)(1+\Phi) \\ &= \Phi' + \Phi_{,i}\, n^i\end{aligned} \tag{3.109}$$

which we can use to substitute for $\Phi_{,i}\, n^i$ into Equation 3.108 to get

$$\frac{1}{p}\frac{\mathrm{d}p}{\mathrm{d}\eta} = -\frac{\mathrm{d}\Phi}{\mathrm{d}\eta} - \mathcal{H} + \Psi' + \Phi' \tag{3.110}$$

We can integrate both sides over $\mathrm{d}\eta$ which will give the relative perturbation of photon energy which is equal to the relative temperature perturbation for blackbody photons

$$\frac{\delta T}{T} = \frac{\delta p}{p} = \Phi(\mathbf{x}_{lss}) - \Phi(\mathbf{x}_0) + \int_{\eta_{lss}}^{\eta_0} (-\mathcal{H} + \Psi' + \Phi')\mathrm{d}\eta \tag{3.111}$$

where the subscript lss denotes the last scattering surface of photons. To solve this requires the initial conditions of perturbations and how they evolved in time.

4 Conclusion

4.1 Summary

In this dissertation, we discussed the basic parameters of the Cosmic Microwave Background: from why it forms, when it forms and considered how you could go about understanding the anisotopies within.

We began by understanding the cause of the CMB: hydrogen recombination which drives the ionisation fraction down and thereby accelerating the freeze-out of interactions of light and matter. When the lowest energy interaction (Thomson scattering) freezes out, light decouples from matter and travels freely across the universe until observed.

We first considered the most basic model of cosmic hydrogen recombination in the Saha model. This assumed recombination directly to ground state in equilibrium conditions and predicted freeze-out to be at $z = 1124$. The main issue with this model was that it assumed recombination directly to ground state hydrogen, a highly unlikely event in the context of the era of the formation of the CMB. Instead we would expect most recombination to occur to the $n = 2$ state before decaying to ground state via either Lyman-α transition or spontaneous two-photon decay.

Considering these additional conditions, we derived a new equation for the evolution of the ionisation fraction and analysed the terms within the equation and whether certain approximations made by sources were valid within the context of CMB formation. We expected the ionisation fraction to fall slower than the Saha equation as any recombination directly to ground state would produce an ionising photon which would immediately ionise any nearby neutral hydrogen atom.

We calculated the rate of recombination to $n = 2$ states and derived the equation for the ionisation fraction under those conditions. The numerical solution to this equation was indeed slower than the Saha equation but proved to be so slow that it did not follow the solution generated by CAMB. Our solution expected the formation of the CMB to occur at $z = 743.4$.

We then attempted to move on to the perturbations within the CMB. Observa-

tional data of the CMB shows that while it is largely isotropic, there exists small perturbations which are due to the effects of primordial perturbations from background parameters of the universe. While the project initially started off with the goal of describing the perturbations of the CMB, due to the discrepancy between the derived ionisation fraction and the graph generated by CAMB, most of the time devoted to the project was spent on looking at the conditions of the ionisation fraction equation and therefore, not enough progress was made on the perturbation theory front.

However, this dissertation does manage to derive the Sachs-Wolfe effect in Newtonian gauge which is the perturbations on the photon energy due to perturbations in the gravitational field.

4.2 Reflection

While we did derive an equation for the evolution of the ionisation fraction, it appeared to deviate significantly from what is expected from CAMB simulations. It may potentially be due to the numerical method used to solve the differential equation or there may be a key piece of physics that I neglected in the derivation. It would be prudent to have greater understanding of particle interactions if I were to return to solving the ionisation fraction equation.

As for the cosmological perturbation theory, there was not enough time personally to go into any sort of depth on the matter. While it is important to have a firm understanding of the foundations, it may have been wiser to simply use results to carry out more productive work rather than reproducing the derivations of the basics of perturbation theory. Especially with the limited time frame which had been allocated to this section somewhat out of necessity (due to the issues around the ionisation fraction).

Bibliography

CAMB Documentation. https://camb.readthedocs.io/en/latest/.

Notes on Photoionized Regions, January 2011. http://www.tapir.caltech.edu/~chirata/ay102/Photoionized.pdf.

Gaussian Units, 2022. http://people.uncw.edu/hermanr/qm/G_units.pdf.

Arfken, G. B. and Weber, H. J. *Mathematical methods for physicists 6th ed.* 2005.

Balkenhol, L., Dutcher, D., Spurio Mancini, A., Doussot, A., Benabed, K., Galli, S., Ade, P. A. R., Anderson, A. J., Ansarinejad, B., Archipley, M., Bender, A. N., Benson, B. A., Bianchini, F., Bleem, L. E., Bouchet, F. R., Bryant, L., Camphuis, E., Carlstrom, J. E., Cecil, T. W., Chang, C. L., Chaubal, P., Chichura, P. M., Chou, T. L., Coerver, A., Crawford, T. M., Cukierman, A., Daley, C., de Haan, T., Dibert, K. R., Dobbs, M. A., Everett, W., Feng, C., Ferguson, K. R., Foster, A., Gambrel, A. E., Gardner, R. W., Goeckner-Wald, N., Gualtieri, R., Guidi, F., Guns, S., Halverson, N. W., Hivon, E., Holder, G. P., Holzapfel, W. L., Hood, J. C., Huang, N., Knox, L., Korman, M., Kuo, C. L., Lee, A. T., Lowitz, A. E., Lu, C., Millea, M., Montgomery, J., Nakato, Y., Natoli, T., Noble, G. I., Novosad, V., Omori, Y., Padin, S., Pan, Z., Paschos, P., Prabhu, K., Quan, W., Rahimi, M., Rahlin, A., Reichardt, C. L., Rouble, M., Ruhl, J. E., Schiappucci, E., Smecher, G., Sobrin, J. A., Stark, A. A., Stephen, J., Suzuki, A., Tandoi, C., Thompson, K. L., Thorne, B., Tucker, C., Umilta, C., Vieira, J. D., Wang, G., Whitehorn, N., Wu, W. L. K., Yefremenko, V., Young, M. R., and Zebrowski, J. A. A Measurement of the CMB Temperature Power Spectrum and Constraints on Cosmology from the SPT-3G 2018 TT/TE/EE Data Set. *arXiv e-prints*, art. arXiv:2212.05642, Dec. 2022. doi: 10.48550/arXiv.2212.05642.

Belušević, R. *Relativity, Astrophysics and Cosmology, 2 Volume Set.* 2008.

Brout, D., Scolnic, D., Popovic, B., Riess, A. G., Carr, A., Zuntz, J., Kessler, R., Davis, T. M., Hinton, S., Jones, D., Kenworthy, W. D., Peterson, E. R., Said, K., Taylor, G., Ali, N., Armstrong, P., Charvu, P., Dwomoh, A., Meldorf, C., Palmese, A., Qu, H., Rose, B. M., Sanchez, B., Stubbs, C. W., Vincenzi, M., Wood, C. M., Brown, P. J., Chen, R., Chambers, K., Coulter, D. A., Dai, M., Dimitriadis, G., Filippenko, A. V., Foley, R. J., Jha, S. W., Kelsey, L., Kirshner, R. P., Möller, A., Muir, J., Nadathur, S., Pan, Y.-C., Rest, A., Rojas-Bravo, C., Sako, M., Siebert, M. R., Smith, M., Stahl, B. E., and Wiseman, P. The Pantheon+ Analysis: Cosmological Constraints. *ApJ*, 938(2):110, Oct. 2022. doi: 10.3847/1538-4357/ac8e04.

Groom, D. E. 2. Astrophysical Constants and Parameters. https://pdg.lbl.gov/2014/reviews/rpp2014-rev-astrophysical-constants.pdf.

Kurki-Suonio, H. Cosmological Perturbation Theory I, January 2022. http://www.courses.physics.helsinki.fi/teor/cpt/CosPer.pdf.

Malik, K. A. Physical Cosmology - SPA6311, December 2022.

Malik, K. A. Advanced Cosmology - SPA7028, April 2023.

Padmanabhan, T. *Theoretical Astrophysics - Volume 1, Astrophysical Processes*, volume 1. 2000. doi: 10.2277/0521562406.

Padmanabhan, T. *Theoretical Astrophysics - Volume 3, Galaxies and Cosmology*, volume 3. 2002. doi: 10.2277/0521562422.

Padmanabhan, T. Advanced Topics in Cosmology: A Pedagogical Introduction. In Daflon, S., Alcaniz, J., Telles, E., and de la Reza, R., editors, *Graduate School in Astronomy: X*, volume 843 of *American Institute of Physics Conference Series*, pages 111–166, June 2006. doi: 10.1063/1.2219327.

Palmer, C. Approximating Sums of Infinite Series, January 1998. http://www.math.wpi.edu/Course_Materials/MA1023C98/infinite/node1.html.

Pritchard, J. R. PHYS97015 Cosmology: Lecture Notes, 2016.

Riess, A. G., Casertano, S., Yuan, W., Bowers, J. B., Macri, L., Zinn, J. C., and Scolnic, D. Cosmic Distances Calibrated to 1% Precision with Gaia EDR3 Parallaxes and Hubble Space Telescope Photometry of 75 Milky Way Cepheids Confirm Tension with ΛCDM. *ApJ*, 908(1):L6, Feb. 2021. doi: 10.3847/2041-8213/abdbaf.

Wascko, M. PHYS60001: Nuclear & Particle Physics Lecture 2 - Tools of the Trade, October 2021.